The Plant Cell, Vol. 16, 1446–1465, June 2004, www.plantcell.org © 2004 American Society of Plant Biologists

Silencing of Hydroxycinnamoyl-Coenzyme A Shikimate/Quinate Hydroxycinnamoyltransferase Affects Phenylpropanoid Biosynthesis [W]

Laurent Hoffmann,[a] Sébastien Besseau,[a] Pierrette Geoffroy,[a] Christophe Ritzenthaler,[a] Denise Meyer,[a] Catherine Lapierre,[b] Brigitte Pollet,[b] and Michel Legrand[a,1]

[a] Institut de Biologie Moléculaire des Plantes, Unité Propre de Recherche, 2357 du Centre National de la Recherche Scientifique, Université Louis Pasteur, 67000 Strasbourg, France

[b] Laboratoire de Chimie Biologique, Unité Mixte de Recherche 206, Institut National de la Recherche Agronomique-Institut National Agronomique, 78850 Thiverval-Grignon, France

The hydroxyl group in the 3-position of the phenylpropanoid compounds is introduced at the level of coumarate shikimate/quinate esters, whose synthesis implicates an acyltransferase activity. Specific antibodies raised against the recombinant tobacco (*Nicotiana tabacum*) acyltransferase revealed the accumulation of the enzyme in stem vascular tissues of tobacco, in accordance with a putative role in lignification. For functional analysis, the acyltransferase gene was silenced in *Arabidopsis thaliana* and *N. benthamiana* by RNA-mediated posttranscriptional gene silencing. In Arabidopsis, gene silencing resulted in a dwarf phenotype and changes in lignin composition as indicated by histochemical staining. An in-depth study of silenced *N. benthamiana* plants by immunological, histochemical, and chemical methods revealed the impact of acyltransferase silencing on soluble phenylpropanoids and lignin content and composition. In particular, a decrease in syringyl units and an increase in *p*-hydroxyphenyl units were recorded. Enzyme immunolocalization by confocal microscopy showed a correlation between enzyme accumulation levels and lignin composition in vascular cells. These results demonstrate the function of the acyltransferase in phenylpropanoid biosynthesis.

INTRODUCTION

Plants represent an important part of the human diet, mainly as a source of energy, vitamins, minerals, fibers, and antioxidants. Among the myriad of plant natural products, compounds issuing from the phenylpropanoid pathway (Figure 1) have been reported to have antioxidant effects, estrogen-like and vasodilatation activities, and anti-inflammatory and anticancer chemopreventive action (Jang et al., 1997; Kahkonen et al., 1999; Burns et al., 2000; Lekse et al., 2001; Stacewicz-Sapuntzakis et al., 2001; Bandoniene and Murkovic, 2002; Boveris et al., 2002; Dixon and Ferreira, 2002). Phenols are ingested in large quantities, for example, from fruits (Stacewicz-Sapuntzakis et al., 2001; Bandoniene and Murkovic, 2002), wine (Jang et al., 1997; Boveris et al., 2002), and coffee (Olthof et al., 2001) and are thought to provide many of the health benefits associated with the consumption of plant foods.

In plants, phenylpropanoids fulfil a vast array of important functions, being involved in development and interactions with the environment (Croteau et al., 2000). For example, stilbenes, coumarins, and isoflavonoids are phytoalexins produced by diseased plants, flavonoids serve as UV irradiation protectants and signals in interactions with symbionts, and acetosyringone and salicylic acid are involved in plant–pathogen interactions. The phenylpropanoid metabolic pathway starts with Phe (Figure 1) and provides, in addition to the products mentioned above, the precursors of lignin, which is quantitatively the second biopolymer on earth after cellulose. Lignin is a major component of the plant cell wall and provides mechanical strength to tree trunks and impermeability to vascular tissues (Lewis, 1999; Humphreys and Chapple, 2002).

Major progress has been made recently in the understanding of the phenylpropanoid biosynthesis pathway (Schoch et al., 2001; Franke et al., 2002a, 2002b; Humphreys and Chapple, 2002; Hoffmann et al., 2003). Although free hydroxycinnamic acids have long been thought to be key intermediates, it is now clearly established that many enzymatic conversions in fact occur instead at the level of hydroxycinnamic esters, aldehydes, and alcohols. Most recent breakthroughs concern the hydroxylation at the 3-position of the aromatic ring, which has been shown to be catalyzed by a cytochrome P450 enzyme (Schoch et al., 2001; Franke et al., 2002a, 2002b). The *Arabidopsis thaliana* 3-hydroxylase (C3H) accepts the shikimate and quinate esters of *p*-coumarate as substrates but not the free acid form or *p*-coumaroyl CoA (Schoch et al., 2001). Arabidopsis mutants targeted in the C3H gene have a reduced epidermal fluorescence phenotype because of the inhibition of sinapoylmalate

[1] To whom correspondence should be addressed. E-mail michel.legrand@ibmp-ulp.u-strasbg.fr; fax 33 388 614442.
The author responsible for distribution of materials integral to the findings presented in this article in accordance with the policy described in the Instructions for Authors (www.plantcell.org) is: Michel Legrand (michel.legrand@ibmp-ulp.u-strasbg.fr).
[W] Online version contains Web-only data.
Article, publication date, and citation information can be found at www.plantcell.org/cgi/doi/10.1105/tpc.020297.

accumulation (Figure 1), accumulate *p*-coumarate esters, and deposit an unusual lignin (Franke et al., 2002a, 2002b), thus indicating that *p*-coumarate esters are probably committed intermediates in the phenylpropanoid pathway. Although the 3-hydroxylation of shikimate and quinate esters of *p*-coumarate by P450 enzymes has been reported earlier (Heller and Kuhnl, 1985; Kuhnl et al., 1987), the acyltransferase that catalyzes the formation of C3H substrates has been characterized only recently (Hoffmann et al., 2003). It uses *p*-coumaroyl CoA as acyl donor and shikimic acid or quinic acid as acceptor, yielding the shikimate or quinate ester, respectively. The acyltransferase has also been shown to catalyze the reverse reaction; that is, transfer of the caffeoyl moiety of 5-*O*-caffeoylquinate onto coenzyme A leading to caffeoyl CoA, the precursor of guaiacyl and syringyl units of lignin (Figure 1). Thus, this enzyme, named hydroxycinnamoyl-CoA shikimate/quinate hydroxycinnamoyltransferase (HCT), appears to be potentially implicated in the pathway both upstream and downstream of the 3-hydroxylation step.

Here, we report on the immunolocalization of tobacco (*Nicotiana tabacum*) HCT and show that it is actively expressed in vascular tissues, in agreement with a putative role in lignin biosynthesis. To ascertain the precise function of HCT in planta, we used RNA-mediated gene silencing to inhibit HCT accumulation in both Arabidopsis and *N. benthamiana* (Smith et al., 2000; Ratcliff et al., 2001). In both systems, plants deficient for HCT function were affected in development and lignin biosynthesis. Whereas Arabidopsis plants were arrested at an early stage of development, the availability of large amounts of silenced tissue from infected *N. benthamiana* permitted a detailed study of the impact of HCT silencing on phenylpropanoid metabolism by immunological, histochemical, and chemical methods. Compared with controls, Klason lignin was decreased by 15% in silenced stems, and the lignin polymer was enriched in hydroxyphenyl (H) units, whereas the proportion of dimethoxylated syringyl (S) units was decreased. HCT immunolocalization and lignin fluorescence were compared in stem sections of control and HCT-silenced plants by confocal laser scanning microscopy. Combined with histochemical staining of lignin, the observations revealed a strict correlation between the level of HCT accumulation and the nature of the lignin. Moreover, the pools of caffeoylquinate isomers were differently affected in stem and leaf tissues of HCT-silenced plants. Taken together, these results demonstrate that HCT plays a critical role in the phenylpropanoid biosynthetic pathway.

RESULTS

Obtention of an Antiserum Specific for Tobacco HCT

The tobacco HCT protein (Hoffmann et al., 2003) was expressed in *Escherichia coli* cells as a fusion protein with glutathione *S*-transferase (GST) (Figure 2A, lane 1). After affinity purification on glutathione beads, the GST tag was cleaved to yield the purified HCT protein (Figure 2A, lane 2). The protein preparation was then injected into rabbits to raise polyclonal antibodies. The antiserum was used in immunoblotting experiments to probe protein extracts from tobacco stems and revealed one major protein with a molecular mass similar to that of the recombinant protein (i.e., 51 kD) (Figure 2A, lane 3). When the antibodies were preincubated in the presence of purified recombinant protein, subsequent recognition of the 51-kD band was strongly inhibited (Figure 2A, lane 4), demonstrating that the polyclonal antibodies specifically recognize the HCT protein in the plant extract. HCT activity was assayed by incubating the same plant extracts with (Figure 2D) or without (Figure 2C) *p*-coumaroyl CoA and shikimate as substrates and by quantifying the reaction product by HPLC. After incubation in the presence of the substrates (not detected in the HPLC profiles of Figure 2D), a major peak appeared that was identified as *p*-coumaroylshikimate by its retention time and UV spectrum (Figure 2D). The minor peak eluting just before (Figure 2D) displayed the same spectrum and is another *p*-coumaroylshikimate isomer. When the antiserum was added to the incubation medium, enzyme activity was completely eliminated from the supernatant after centrifugation in the presence of protein A–Sepharose, whereas the preimmune serum had no effect in the same conditions (Figure 2B). These data demonstrate that the protein specifically recognized by the antibodies (Figure 2A) has HCT activity.

Study of HCT Expression in Tobacco

HCT expression in different tobacco tissues was investigated in immunoblotting experiments (Figure 3A). The strongest signals were observed with extracts from internodes of tobacco stems (Figure 3A, lane 1). Lower levels of expression were detected in roots and petioles (Figure 3A, lanes 2 and 3), whereas only faint bands were detected in extracts from different flower tissues (Figure 3A, lanes 4 to 6). Finally, the level of expression in leaves was below the detection limits of the immunological method (Figure 3A, lanes 7 and 8). The same protein extracts were assayed for acyltransferase activity by incubating plant extracts in the presence of the two substrates and quantifying the *p*-coumaroylshikimate peak after HPLC, as illustrated in Figure 2. The method proved highly sensitive because even the low activity present in leaves could be accurately measured (Figure 3B). Moreover, these results illustrate that there is a high level of expression of HCT in lignified tissues, such as stems and roots, and show a good correlation between the amounts of HCT protein and the levels of HCT activity.

To further address the putative role of HCT in lignin biosynthesis, we investigated the localization of HCT in lignifying tissues in comparison with that of a typical lignification enzyme, caffeoyl-CoA *O*-methyltransferase (CCoAOMT) (Figure 4). The tissues were observed either by epifluorescence microscopy (Figures 4A to 4F) at different excitation/emission wavelengths (see Methods) to reveal Alexa 568 immunolabeling (Figures 4A to 4C) and lignin autofluorescence (Figures 4D to 4F) or under bright-field conditions to reveal the anatomy of the tissues (Figures 4G to 4I). All images were acquired using the same exposure time to allow comparison between the different panels. The top panels of Figure 4 present serial thin sections of tobacco stems that have been incubated with antisera directed against the HCT protein (Figure 4A), the CCoAOMT protein (Figure 4B), or with a preimmune serum (Figure 4C). Only a very low signal was

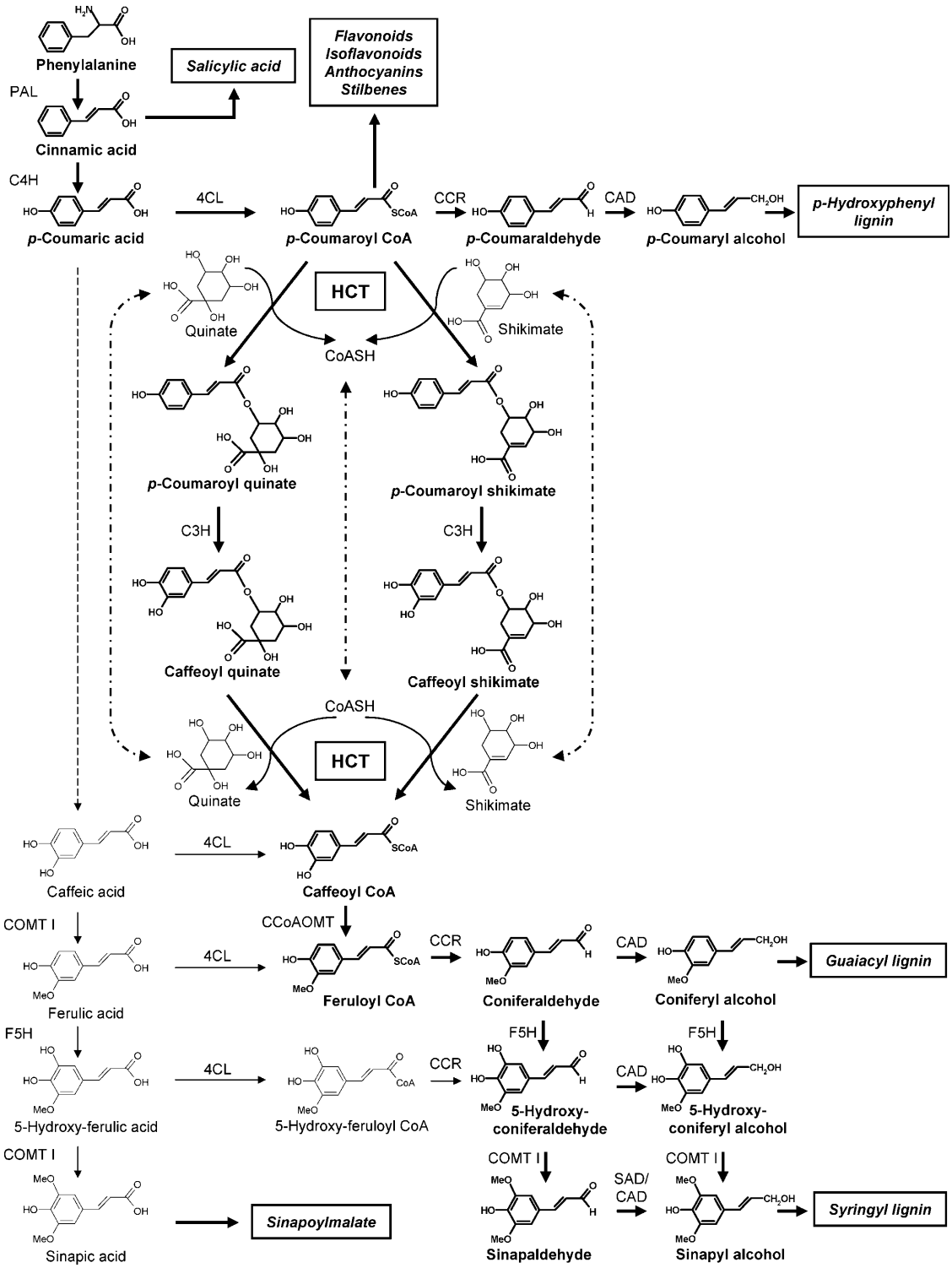

Figure 1. A Current View of Phenylpropanoid Metabolism.

Route to lignin subunits and major products is shown in bold. The double-headed arrows illustrate coenzyme A (CoASH), quinate, and shikimate recycling after the 3-hydroxylation step. 4CL, 4-hydroxycinnamoyl-CoA ligase; C3H, *p*-coumarate 3-hydroxylase; C4H, cinnamate 4-hydroxylase; CAD, cinnamyl-alcohol dehydrogenase; CCoAOMT, caffeoyl-CoA *O*-methyltransferase; CCR, cinnamoyl-CoA reductase; COMT I, caffeic/5-hydroxyferulic acid *O*-methyltransferase; F5H, ferulate 5-hydroxylase; HCT, hydroxycinnamoyltransferase; PAL, Phe ammonia-lyase; SAD, sinapyl-alcohol dehydrogenase.

observed in the sample treated with the preimmune serum (Figure 4C) or when the serum was preincubated in the presence of purified recombinant HCT protein (see supplemental data online). This low background colocalized with lignified xylem cells (compare Figure 4C to the intense autofluorescence generated by the accumulation of phenolic polymers within the walls of the xylem tracheid elements in Figure 4F) and was also detected when the secondary antibody was omitted (data not shown). The background signal is therefore likely to be because of the weak autofluorescence of lignin at excitation wavelength of 515 to 565 nm and emission wavelength of 582.5 to 627.5 nm. In contrast with the preimmune control, strong labeling was observed with specific sera raised against HCT (Figure 4A) or CCoAOMT (Figure 4B). In the case of HCT, the signal was mainly localized within the external and inner phloem cells (white arrowheads) and to a lesser extent in the cambium zone. When compared with the background detected in xylem with the preimmune serum (Figure 4C), the signal detected in xylem with the anti-HCT serum (Figure 4A) was low but significant. This is in contrast with the CCoAOMT labeling, which was mainly localized in the young xylem cells that are actively lignifying (Figure 4B, yellow arrowheads), and to a lesser extent in association with the older xylem cells situated beneath. This localization of CCoAOMT is in agreement with the activity of the enzyme, which catalyzes the synthesis of feruloyl CoA, the precursor of both guaiacyl and syringyl subunits of lignin that are deposited in xylem tracheids. As for HCT, CCoAOMT labeling was also detected in internal and external phloem cells (Figure 4B, white arrowheads), but almost

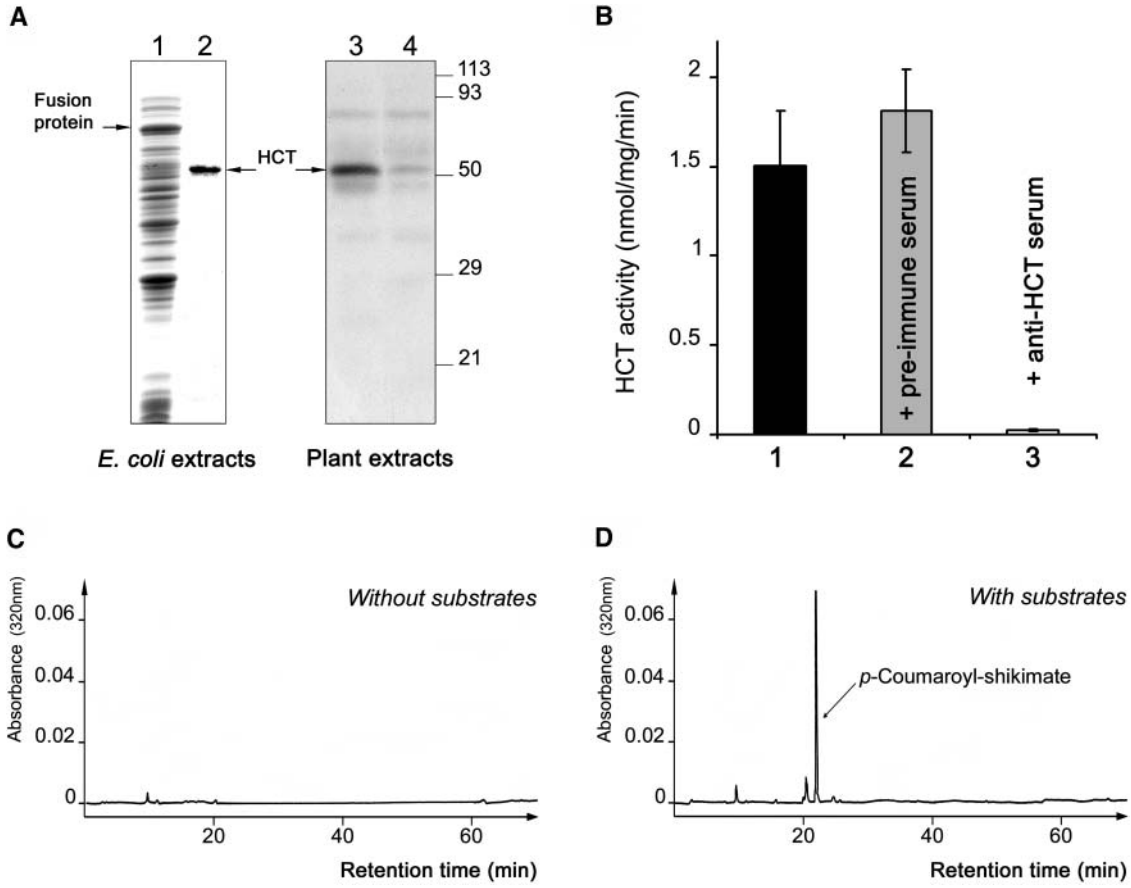

Figure 2. Specific Antibodies Raised against the Recombinant Protein Inhibit HCT Activity Measured in Plant Extracts by HPLC Analysis of Reaction Products.

(A) The tobacco HCT clone was expressed in *E. coli* cells and the GST-HCT fusion protein (arrow in lane 1), affinity-purified, and cleaved to yield the purified recombinant protein (arrow in lane 2) for injection into rabbits. A crude protein extract (3 μg) from tobacco stems was immunoblotted with the anti-HCT polyclonal antiserum (lane 3) or with a serum aliquot that had been incubated in the presence of the purified recombinant HCT protein (lane 4; see Methods). The arrows indicate the position of GST-HCT fusion and HCT proteins. At the right is the position of markers of known molecular mass (given in kD).

(B) Immunoprecipitation studies. HCT activity was measured in the absence of serum (1) or in the presence of preimmune (2) or anti-HCT serum (3; see Methods) after centrifugation with protein A–Sepharose.

(C) HPLC analysis of a plant extract after incubation in the absence of substrates.

(D) After incubation in the presence of *p*-coumaroyl-CoA and shikimate as substrates, the amount of *p*-coumaroylshikimate was estimated by HPLC and taken as a measurement of HCT activity.

no signal was present within the cambium zone from which the xylem cells differentiate. No signal was found in cortex and pith tissues with either serum. Thus, it appears that the distribution of HCT and CCoAOMT in vascular tissues is not identical, despite their proximity in the lignin biosynthetic scheme (Figure 1).

Effects of HCT Gene Repression by RNA Silencing in Arabidopsis

A gene of Arabidopsis (At5g48930) has been cloned previously and shown to encode an acyltransferase with catalytic activity similar to that of tobacco HCT (Hoffmann et al., 2003). The Arabidopsis enzyme, as tobacco HCT, accepts *p*-coumaroyl CoA and caffeoyl CoA as substrates and transfers the acyl group on both shikimate and quinate acceptors (data not shown). Transgenic Arabidopsis carrying a hairpin repeat of a portion of the HCT sequence (At5g48930) was produced (see Methods) to obtain plants in which HCT accumulation was inhibited by RNA-mediated posttranscriptional gene silencing. Transgenic plants were selected for their resistance to Basta, and 300 transformants were obtained from ~30,000 seeds. They displayed severely reduced growth and dark green/purple leaves as compared with wild-type controls (Figure 5A). Among them, a large majority (97%) did not develop a floral stem (plant i, Figure 5A), and ~10 had a short stem (plants ii and iii in Figure 5A) but were also sterile. RNA gel blot analysis performed on pools of 70 plants demonstrated the degradation of HCT mRNA (Figure 5B, top panel) and the appearance of siRNAs (Figure 5B, middle panel) in transgenic plants compared with controls. Consistently, the HCT activity measured in two distinct samples of HCT-silenced plants was ~1% of the wild-type value (Figure 5C). The impact of HCT gene repression on lignification of the floral stem of plant iii (Figure 5A) was evaluated by histochemical methods. Lignin was revealed by Wiesner staining in interfascicular fibers and in xylem bundles of wild-type and transgenic stems (Figure 5D). In the latter, some changes in the coloration were revealed, maybe because of changes in lignin composition, and alterations in the anatomy of the interfascicular tissues and xylem bundles were observed. Maüle coloration, which is specific for S units of lignin (dimethoxylated units, Figure 1), stained interfascicular fibers of wild-type stem section, whereas no staining was detected in silenced tissues (Figure 5D). This observation suggests that the Arabidopsis mutant is poor in S lignin because of *HCT* gene repression.

Virus-Induced *HCT* Silencing Affects *N. benthamiana* Plant Development

The severe dwarf phenotype and sterility because of *HCT* silencing in Arabidopsis prevented an in-depth study of the impact of low HCT levels on the lignin polymer using chemical methods that require substantial amounts of material. Therefore, we used a tobacco rattle virus (TRV)-based virus-induced gene silencing (VIGS) system to repress *HCT* gene expression in *N. benthamiana*.

We have shown previously that tobacco HCT belongs to the BADH family of acyltransferases (St-Pierre and De Luca, 2000; Hoffmann et al., 2003). A partial HCT cDNA from *N. benthamiana* was cloned by RT-PCR using primers designed from conserved sequences in the BADH gene family (see Methods). A 957-bp fragment was isolated that shared 96% homology with the tobacco HCT cDNA (data not shown) and was used as a probe to analyze genomic DNA of *N. benthamiana* by DNA gel blotting (Figure 6A). Restriction of the plant DNA with *Eco*RI (one site in

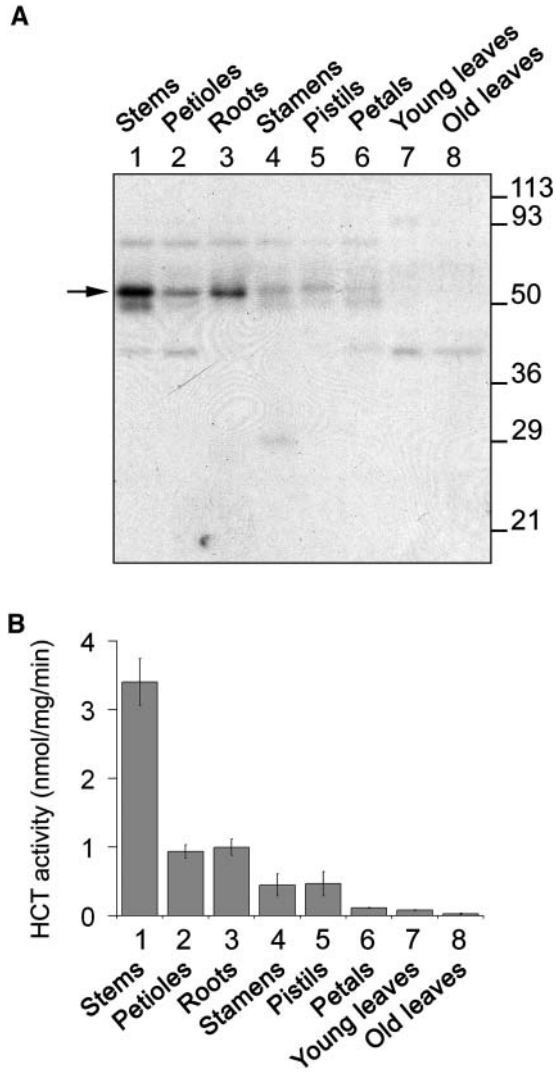

Figure 3. HCT Expression in Different Tissues of *N. tabacum* Plants.

(A) Protein extracts prepared from different plant tissues were analyzed by electrophoresis on SDS-polyacrylamide gels and immunodetected with polyclonal antibodies raised against the purified recombinant protein. Expression levels in stems (lane 1), petioles (lane 2), roots (lane 3), stamens (lane 4), pistils (lane 5), petals (lane 6), and young and old leaves (lanes 7 and 8, respectively) were compared. The arrow indicates the migration of the HCT protein, and at the right is the position of markers of known molecular mass (given in kD).

(B) The amount of *p*-coumaroyl-shikimate formed upon incubation was used to calculate HCT activity in the different extracts analyzed in **(A)**. Mean values and standard errors were calculated from three independent experiments.

the gene coding sequence) or *Kpn*I (no sites) indicated that only one copy of *HCT* is present in the *N. benthamiana* genome (Figure 6B).

The HCT cDNA fragment was introduced in the TRV vector, and VIGS was used to silence the *N. benthamiana HCT* gene in infected plants. Figure 7 presents the effects of HCT silencing on plant development. As controls (plants at the left in Figure 7), we used plants infected with TRV vector containing an unrelated sequence, the sequence of the green fluorescent protein (GFP). When the TRV vector harbored the HCT sequence, plant development was affected to different extents: phenotypes ranging from no visual phenotype to a severe growth phenotype. In the example shown in Figure 7 (plants at the right), whole plant size was severely reduced (Figures 7A and 7B), and root development was inhibited (Figure 7C). Such phenotypes were never recorded in control plants, totally excluding the possibility that the viral infection was at their origin.

The level of HCT inhibition was first evaluated by immunoblotting in a set of plants differently affected in their development. Figure 8 presents HCT expression compared with CCoAOMT expression in two control plants (C1 and C2) infected with TRV-GFP and in seven plants infected with TRV-HCT. Expression levels were evaluated by immunoblotting protein extracts from stems (Figure 8A) or roots (Figure 8B). In the controls (C1 and C2), HCT protein (top panels) and the two CCoAOMT isoforms (bottom panels) (Maury et al., 1999) were readily detected in stem and root tissues. In tissues of TRV-HCT–infected plants I to VI (Figures 8A and 8B), the HCT protein was barely detectable,

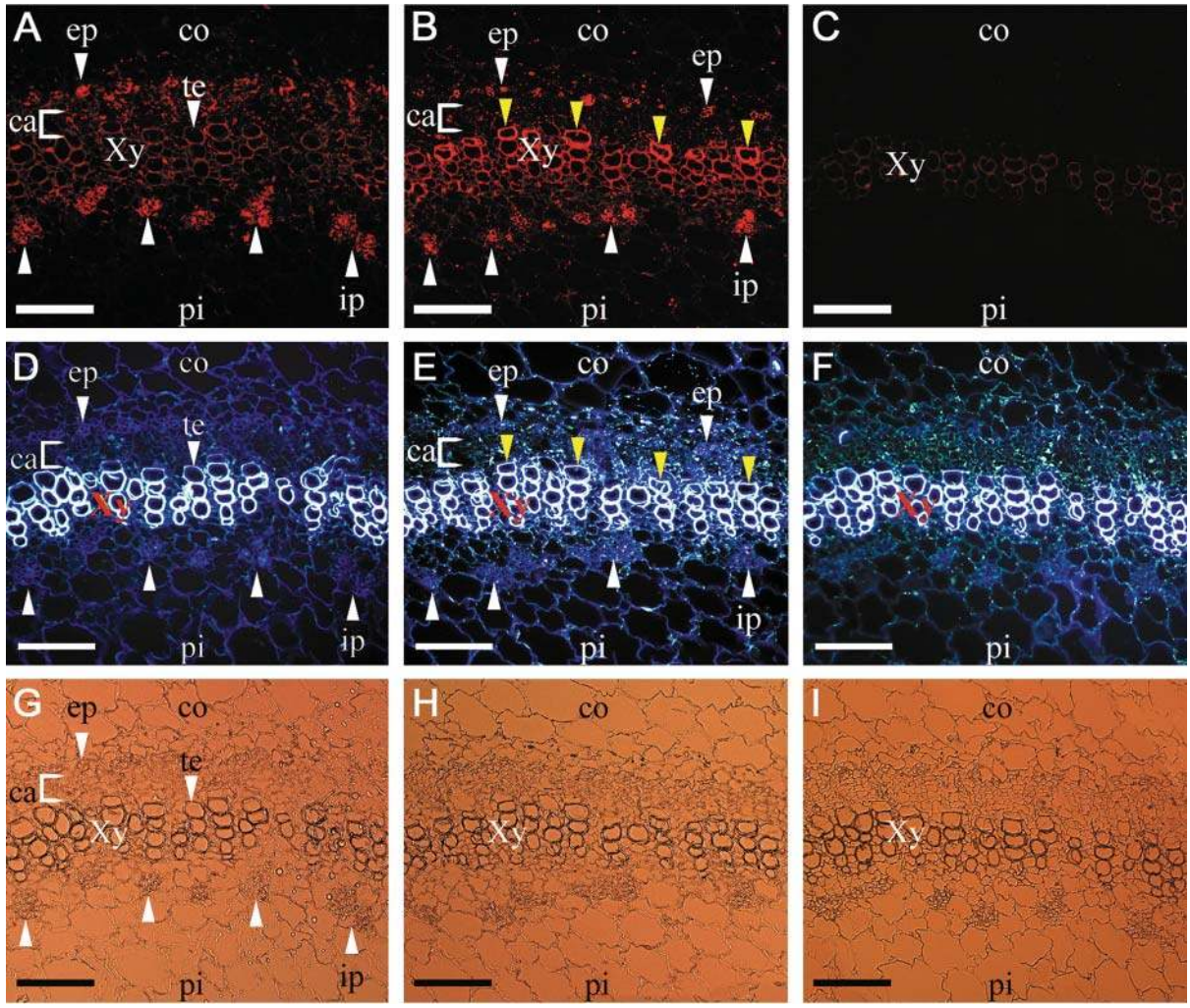

Figure 4. Comparative Immunolocalization of HCT and CCoAOMT in Tobacco Stem Sections.

(A), **(B)**, and **(C)** Immunofluorescence labeling obtained with anti-HCT **(A)**, anti-CCoAOMT **(B)**, and HCT preimmune serum **(C)**.
(D), **(E)**, and **(F)** Autofluorescence corresponding to sections **(A)**, **(B)**, and **(C)**, respectively.
(G), **(H)**, and **(I)** Anatomy of the same tissues sections as observed under bright-field conditions.
ca, cambium; co, cortex; ip, internal phloem; ep, external phloem; pi, pith; te, tracheary element; xy, xylem. Bars = 200 μm. See additional controls in supplemental data online.

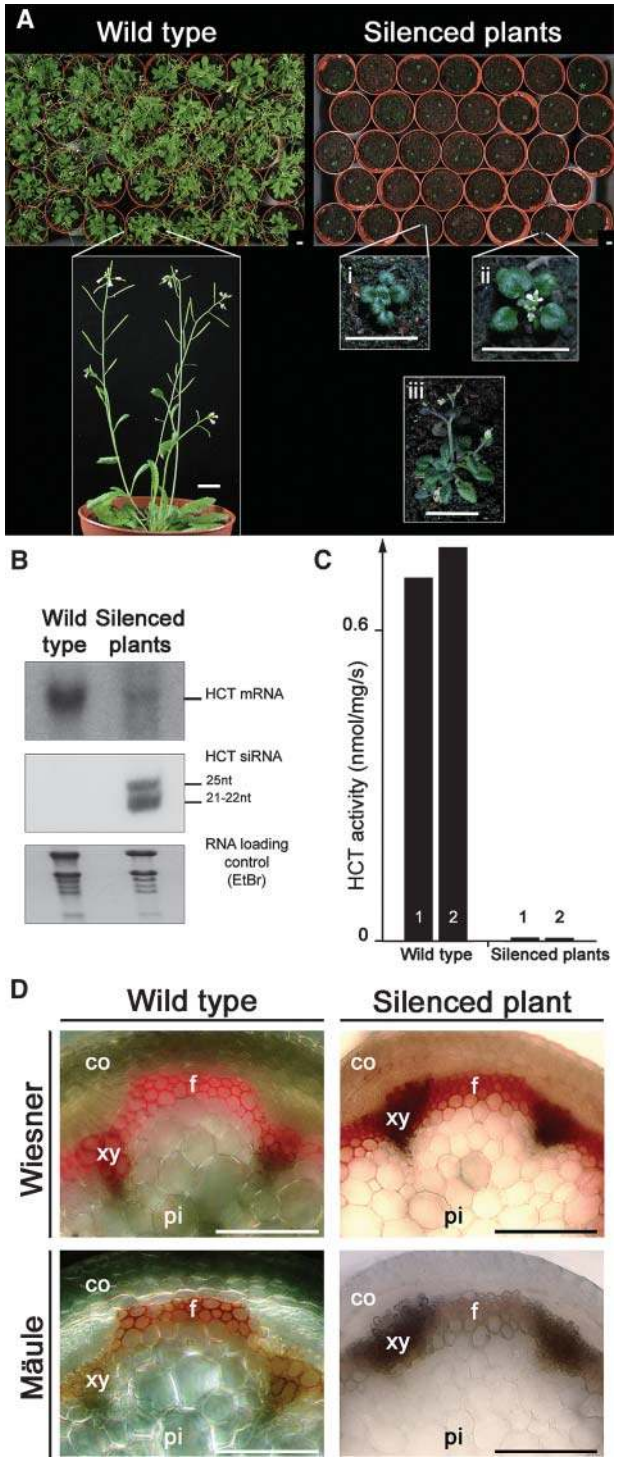

Figure 5. RNA Silencing of HCT in Arabidopsis.

(A) Wild-type (one plant per pot) and HCT-silenced (three plants per pot) Arabidopsis plants at 2 months of age. Bar = 1 cm.

(B) RNA gel blots (8 μg per lane) showing HCT mRNA (top panel) and HCT siRNA (middle panel). Total RNA in the same samples after staining with ethidium bromide (EtBr) is shown in the bottom panel. RNA was extracted from pools of 70 plants. The position of the different RNA species is indicated at the right.

(C) HCT activity in wild-type and HCT-silenced plants measured on two independent batches (lanes 1 and 2) of 50 plants each.

(D) Histochemical staining of lignin of wild-type and HCT-silenced inflorescence stems. Abbreviations are as in Figure 4. f, interfascicular fibers. Bars = 100 μm.

whereas CCoAOMT expression was not affected, in accordance with the specificity of the VIGS phenomenon (Ratcliff et al., 2001). In plant VII, HCT expression was much less reduced, thus indicating that VIGS was less efficient in this particular plant, which showed attenuated developmental defects (data not shown). These data demonstrate the efficiency of HCT silencing in most of the TRV-HCT infected plants and suggest that the amplitude of the impact on plant development is correlated with the extent of *HCT* gene silencing.

Impact of *HCT* Silencing on Lignin Biosynthesis in *N. benthamiana*

Because HCT mainly localizes in lignified tissues (Figures 3, 4, and 8), the effects of *HCT* silencing on lignification of stem and root tissues of TRV-infected *N. benthamiana* plants was evaluated. Figure 9 presents histochemical staining of stem and root sections of plants that have been infected with TRV-GFP or TRV-HCT vectors. In control samples, staining was strong in xylem vascular tissues, appearing as colored rings in stem sections (Figures 9A and 9B) and as colored disks in root tissues (Figures 9C and 9D). Histochemical staining detected changes in the lignification of both stem and root vascular tissues of the TRV-HCT–infected plants. Wiesner staining (reflecting total lignin amount) was significantly affected only in a few cases, as in the sections shown in Figures 9E, 9G, and 9I (arrows), whereas Maüle staining (specific for lignin S units) proved much more sensitive and revealed the appearance of unstained white zones in the xylem tissues of all plants examined (marked by arrows). The youngest outmost tissues were the most affected in stem as well as in root tissues. In the Maüle-stained sections, the extent of the white zones depleted in syringyl units varied between individual plants, as exemplified by plants II, IV, and VII in Figure 9. It is of note that only minor effects on lignin composition were detectable in roots of plant VII (Figure 9P) that was only moderately silenced for HCT (Figure 8) and had no growth phenotype. These histochemical data confirm that *HCT* repression has a direct effect on lignin synthesis.

The impact of *HCT* silencing on lignin structure was further studied by chemical methods. The amount of lignin in 3-month-old plants was estimated by the gravimetric Klason method on stem material after solvent extraction (referred to from now on as extract-free samples). As shown in Table 1, the noninfected and TRV-GFP–infected controls had similar lignin levels. By contrast, lignin accumulation was decreased by 15% in silenced plants, consistent with the relatively small effects observed with the Wiesner stain (Figure 9). Lignin structure was studied by

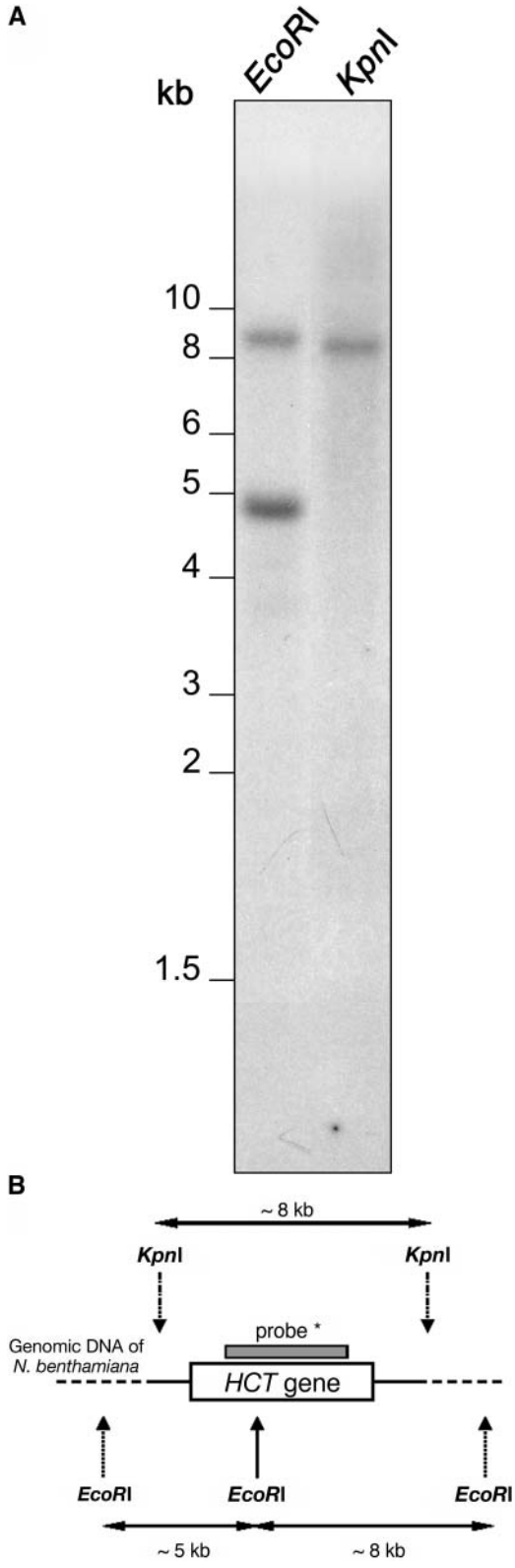

Figure 6. One Copy of the *HCT* Gene Is Present in the *N. benthamiana* Genome.

(A) Gel blot analysis of *Eco*RI- and *Kpn*I-digested genomic DNA (40 μg per lane) probed with the HCT cDNA. The position of length markers is given at the left.

(B) Schematic drawing of the relative position of the HCT coding sequence and *Eco*RI and *Kpn*I restriction sites as inferred from **(A)**.

thioacidolysis degradation, which gives rise to H, G, and S thioethylated lignin-derived monomers from H, G, and S lignin units involved in labile β-*O*-4 ether bonds. Therefore, the total yield of thioacidolysis monomers gives a measure of the proportion of lignin units involved in such bonds. Conversely, this yield is reduced when the proportion of resistant interunit bonds in lignin is high. Table 1 presents the results of thioacidolysis analysis of lignin. The yields revealed that lignin of noninfected and TRV-GFP–infected control samples had ~40% units only involved in β-*O*-4 bonds. By contrast, this percentage was substantially lower (27%) in HCT-silenced plants (Table 1), indicating a more condensed lignin compared with controls. Together with the enrichment in resistant interunit lignin bonds, thioacidolysis revealed that the relative proportions of the main lignin units were markedly altered. As shown in Table 1, when subjected to thioacidolysis the two controls essentially released the G and S monomers (S/G molar ratio of 2.4 for the noninfected sample and 2.3 for the TRV-GFP infected one), whereas the H monomer was recovered as a trace component. By contrast, the latter nonmethoxylated monomer was obtained in substantial relative amounts (8% of the lignin-derived monomers) from the TRV-HCT–infected plants. This relative increase in H monomer did not affect the proportion of G monomer, which was 29 to 30% in all cases, although the S monomer was reduced from 69 to 70% in the controls to 63% in the HCT-silenced plants (Table 1, molar ratio values). This result is in agreement with the fact that large areas of some stem sections did not stain with Maüle reagent (Figure 9). These changes in lignin composition are consistent with the increase of resistance toward thioacidolysis degradation (i.e., a lower proportion of labile β-*O*-4 linkages, Table 1) because the C-5 position of the aromatic ring is available for highly resistant carbon–carbon bonds in the H unit but not in the S unit. Thus, it appears that changes in the lignin structure of silenced plants mainly arise from a decrease in dimethoxylated S units and a concomitant increase in nonmethoxylated H units.

To ascertain that the modifications of the lignin composition observed in the silenced plants correlated with the extent of changes in HCT accumulation, the same stem sections from nonsilenced (TRV-GFP) and silenced (TRV-HCT) *N. benthamiana* plants were immunolabeled using anti-HCT antibodies, analyzed by confocal laser scanning microscopy (CLSM) for labeling and autofluorescence, and then further processed for Maüle staining as illustrated in Figure 10. In TRV-GFP plants, HCT labeling (Figure 10A, red signal) was intense and uniformly distributed within the cambium zone surrounding the strongly autofluorescing xylem cells (Figure 10B). Some HCT labeling was also detected in the xylem cells, as is readily visualized on merged images (Figures 10C and 10M). When observed at higher

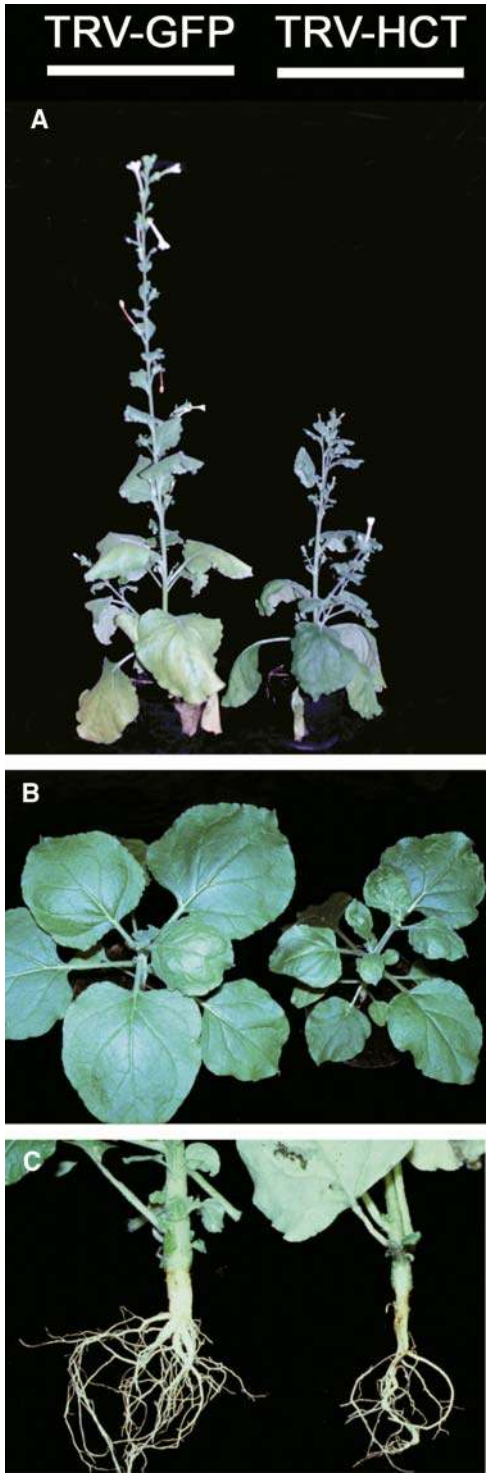

Figure 7. Phenotypes of *N. benthamiana* Plants Subjected to VIGS of the *HCT* Gene.

Impacts on the whole plant size (**[A]** and **[B]**) and root growth **(C)** are shown. At the left in each photograph is a control plant infected with the TRV-GFP vector, and at the right is a plant infected with the TRV-HCT vector.

magnification, HCT labeling was also revealed to radiate within ray cells (arrowheads, Figure 10D). Using the same CLSM settings to allow comparison of the data, overall HCT labeling of silenced plants was faint (Figures 10E and 10G, red signal), and its distribution within the cambium was much less uniform than in control plants (cf. red signal in Figures 10M and 10N). At high magnification, the faint signal within the cambium was better visualized, and almost no labeling was apparent in the xylem ray cells (Figure 10H). Contrary to the nonsilenced plants in which the lignin autofluorescence was rather uniform, silenced plants showed large patches of intensely autofluorescent xylem cells (cf. the green signal intensity in Figures 10B and 10F, 10D and 10H, and 10M and 10N, respectively). In the absence of primary antibody, no red signal was detected at the wavelengths used to reveal Alexa 568 labeling (Figures 10I, 10K, and 10L); only the uniform distribution of the autofluorescence of the xylem cells was visible at the appropriate wavelength (Figures 10J to 10L), confirming the specificity of the HCT antibody.

To further address the extent and nature of lignification that occurred in the samples used for HCT immunolabeling (Figures 10A to 10H), the same stem sections were recovered after CLSM observation and processed for Maüle staining. As shown in Figure 10O and in agreement with previous observations (Figure 9), xylem vascular tissues from nonsilenced plants appeared as uniformly colored rings, whereas those from silenced plants were variegated. Interestingly, the white patches of cells depleted in syringyl units (as indicated by the arrow in Figure 10P) corresponded to the areas where the lignin autofluorescence intensity was the highest and HCT labeling was virtually undetectable (Figure 10N, arrow). Therefore, reduced HCT expression correlated in vivo with reduced lignin syringyl content and increased lignin autofluorescence. It is concluded that lignin biosynthesis depends on HCT activity in vivo, and its reduction by VIGS is most probably at the origin of the altered spectral characteristics of lignin.

Impact on Cell Wall Degradability

We examined the consequences of the changes in lignin content and structure upon the resistance of *N. benthamiana* cell walls to hydrolase activity. The susceptibility of the tissues to cellulase activity was studied, and the results are presented in Table 2. The cell walls of TRV-HCT–infected tissues were degraded to a much higher extent than controls (noninfected and TRV-GFP) because weight loss reached 160% of the control values (Table 2). This was likely the result of facilitated cellulase action in tissues in which lignification had been altered as a result of *HCT* silencing.

Changes in the Accumulation of Caffeoylquinate Isomers in HCT-Silenced Tissues

In view of the upstream position of HCT in the pathway, its repression may affect not only lignin but also other metabolites, in particular soluble compounds. Morever, caffeoylquinate has been shown to be both synthesized and catabolized by HCT (Hoffmann et al., 2003). Figure 11A presents typical HPLC profiles of soluble phenolic compounds extracted from stem tissues of TRV-GFP and TRV-HCT–infected *N. benthamiana*

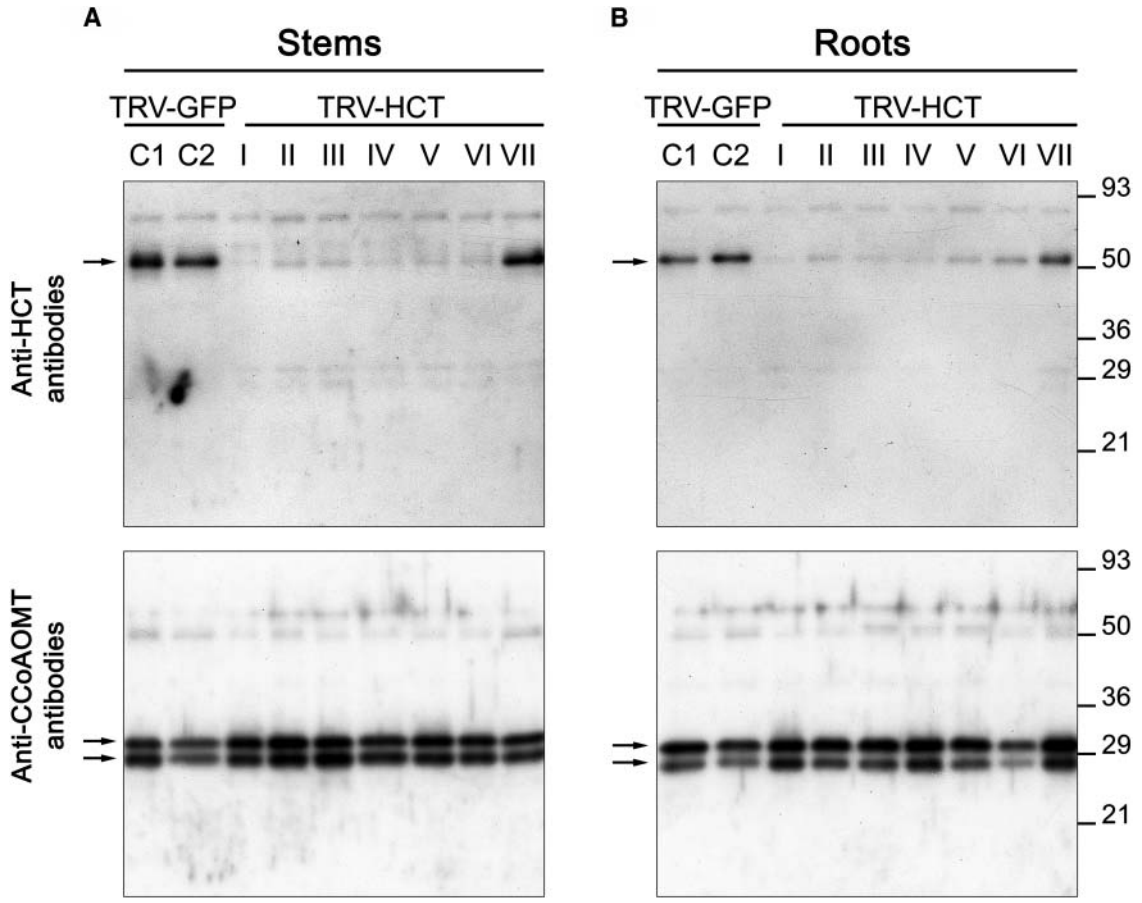

Figure 8. HCT Accumulation in Stem and Root Tissues of TRV-Infected *N. benthamiana* Plants.

Protein extracts (3.5 μg) from stems **(A)** (internode 5) or roots **(B)** were immunodetected with specific antibodies raised against tobacco HCT (top panels) or CCoAOMT (bottom panels) proteins. HCT and CCoAOMT contents of two representative controls (C1 and C2, TRV-GFP) and seven TRV-HCT–infected plants (lanes I to VII) are presented. Arrows indicate the position of HCT (top panels) or CCoAOMT isoforms (bottom panels). At the right is the position of markers of known molecular mass (in kD).

plants. In each chromatogram, three major peaks (marked by arrows in Figure 11A) appeared that displayed identical UV spectra (insets in Figure 11A), characteristic of caffeoylquinic acids. From their relative retention times, the three compounds were identified as 3-, 5-, and 4-caffeoylquinate isomers by comparison with standards (data not shown) (Strack and Gross, 1990). The amounts of the three caffeoylquinate isomers clearly increased in stems upon HCT silencing. When leaf content was examined, important fluctuations in caffeoylquinate amounts were detected (data not shown). Therefore, HCT activity and caffeoylquinate content were estimated in stem and leaf extracts of nine silenced and nonsilenced plants, and the calculated mean values and deviations are presented in Figures 11B and 11C. In control (TRV-GFP) plants, a 60-fold higher HCT activity was measured in stems compared with leaves, similar to what was observed in tobacco (Figure 3B). Gene silencing resulted in ~70 and 40% reduction of HCT activity in stems and leaves, respectively. Concerning the impact on soluble phenolic compounds, the results confirm that the reduction of HCT activity has a differential impact on caffeoylquinate accumulation in the two tissues. In stems, a threefold increase was measured (Figure 11B), whereas no significant change of caffeoylquinate concentration was observed in silenced leaves (Figure 11C). Inspection of other metabolites did not reveal any other important alteration in phenolic profiles as a result of HCT inhibition.

DISCUSSION

The recent characterization of an acyltransferase (HCT) (Hoffmann et al., 2003) capable of synthesizing *p*-coumaroyl shikimate and *p*-coumaroyl quinate esters and of the cytochrome P450 C3H that uses the *p*-coumaroyl esters as substrates (Schoch et al., 2001; Franke et al., 2002a) has profoundly changed our view of the phenylpropanoid biosynthetic pathway (Humphreys and Chapple, 2002). Here, as a first step toward the understanding of the role of HCT in lignin biosynthesis in planta, we have immunolocalized the enzyme in stem vascular tissues of *N. tabacum* and *N. benthamiana*.

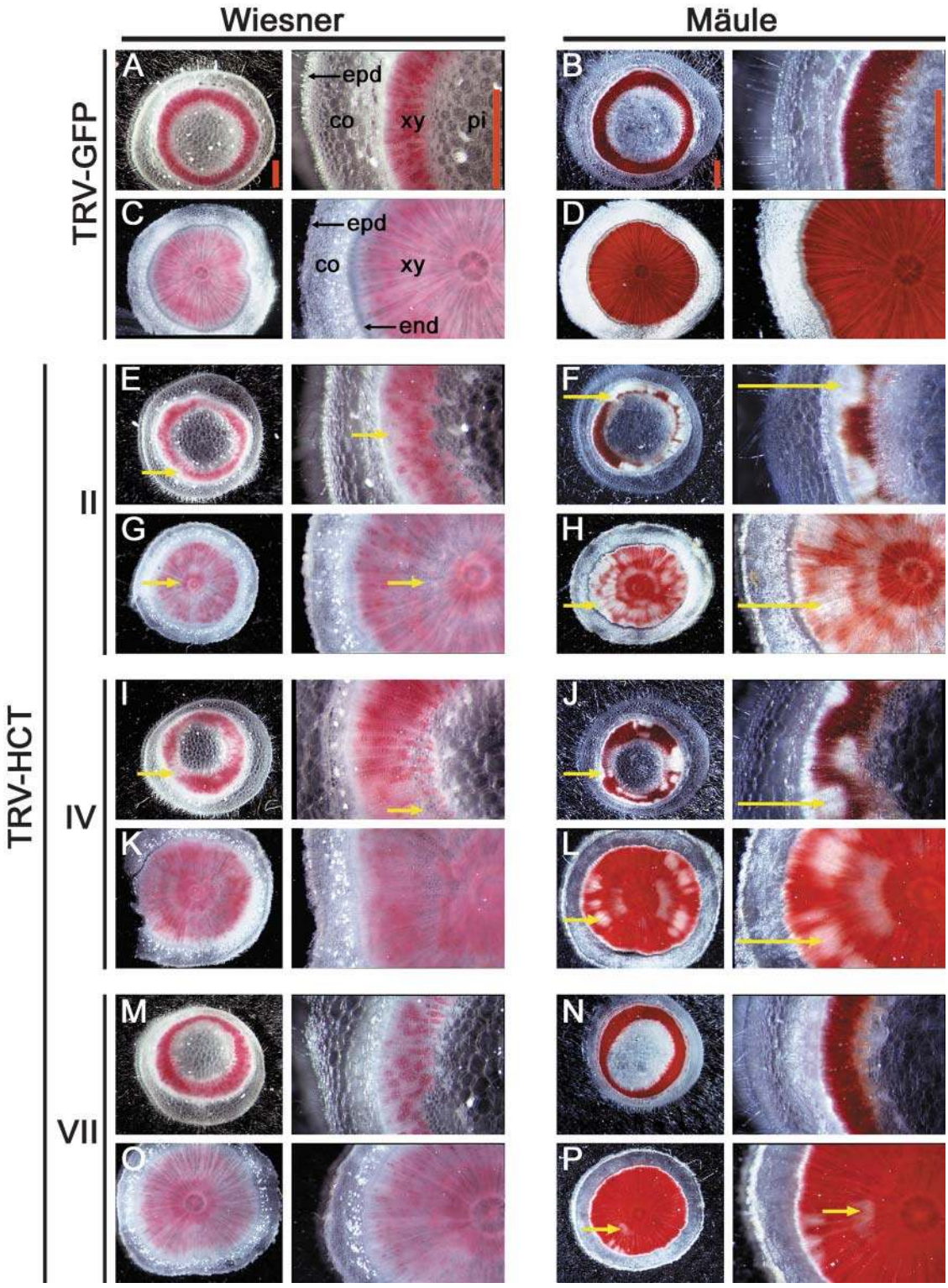

Figure 9. Histochemical Analysis of the Effects of *HCT* Silencing on Lignin of *N. benthamiana*.

Sections of stems (**[A]**, **[B]**, **[E]**, **[F]**, **[I]**, **[J]**, **[M]**, and **[N]**) and roots (**[C]**, **[D]**, **[G]**, **[H]**, **[K]**, **[L]**, **[O]**, and **[P]**) were stained using Wiesner (left panels) or Maüle (right panels) methods. Sections of a representative control (**[A]** to **[D]**), sections from a plant with a strong phenotype (**[E]** to **[H]**), sections from a plant with an intermediate phenotype (**[I]** to **[L]**), and sections of a plant with no visible phenotype (**[M]** to **[P]**) are shown. Arrows indicate zones with attenuated lignin staining. All the pictures in one column are at the same scale (indicated at the top, bars = 1 mm). epd, epidermis; end, endodermis; other abbreviations are as in Figure 4.

Table 1. Effects of *HCT* Silencing on Lignin Content and Structure in 3-Month-Old *N. benthamiana* Stems

	Noninfected	TRV-GFP Infected	TRV-HCT Infected
Klason lignin[a]	10.9 ± 0.3 (100 ± 4)	11.2 ± 0.3 (103 ± 3)	9.32 ± 0.2 (85 ± 2)
Thioacidolysis Yield in H, G, and S Monomers (μmol/g KL)[b]			
H	2.7 ± 0.2	3.7 ± 0.1	85 ± 5
G	426 ± 13	514 ± 19	323 ± 9
S	1033 ± 61	1165 ± 55	683 ± 15
Total (H + G + S)	1462 ± 74	1683 ± 74	1091 ± 29
Molar ratio (H/G/S)	0.2/29.1/70.7	0.2/30.6/69.2	8/29.6/62.6
Percentage of units only involved in β-*O*-4 bonds[c]	37 ± 2	42 ± 2	27 ± 1

[a] Klason lignin is expressed as weight percentage of extract-free sample (mean value and standard error of four replicate analyses). Values in parentheses are relative to uninfected control taken as 100%.

[b] Mean value and standard error of duplicate analyses. The reported standard error includes both the Klason determination (relative standard error in the 2 to 3% range) and the thioacidolysis experiment (relative standard error in the 0.1 to 3% range). KL, Klason lignon.

[c] The percentage of lignin units only involved in β-*O*-4 bonds is calculated with the assumption that the average M_r of lignin units is 200 and that the recovery yield of thioacidolysis monomers from parent β-*O*-4 structures is 80%.

Using a specific antiserum raised against the purified recombinant protein to probe various plant extracts, HCT was shown to accumulate in lignified tissues of stems and roots (Figures 3, 4, 8, and 10). Immunocytochemical localization of HCT in vascular tissues was compared with that of CCoAOMT, which has previously been associated with lignification in various plants (Ye, 1997; Inoue et al., 1998; Maury et al., 1999). Differences in the spatial and temporal enzyme distribution have been demonstrated for CCoAOMT and caffeic/5-hydroxyferulic acid *O*-methyltransferase (COMT) in alfalfa (*Medicago sativa*) and tobacco tissues and may be at the origin of subtle variations in lignin of distinct cell types (Inoue et al., 1998; Maury et al., 1999). The comparative localization of CCoAOMT and HCT in tobacco showed that both enzymes accumulate exclusively in vascular tissues, and no signal was seen in the pith and cortex of stems. HCT protein labeling was particularly strong in inner and external phloem and was also detectable in cambium cells where no signal was recorded with anti-CCoAOMT antibodies (Figure 4). A strong accumulation of HCT was also found in the cambium of *N. benthamiana* (Figure 10). HCT was not clearly detected in differentiating young xylem cells of tobacco, a major site of CCoAOMT accumulation. In *N. benthamiana*, HCT labeling clearly localized in ray cells of xylem tissues (Figure 10). Thus, a distinct spatial repartition of HCT and CCoAOMT was found. This may be related to the relative position of the two lignin biosynthetic enzymes in the pathway (Figure 1) and their participation at different stages of the cell lignification process. However, it cannot be excluded that HCT may play a more specific role, for instance in the mobilization of caffeoylquinate pools that may be transformed in caffeoyl CoA as demonstrated in vitro (Hoffmann et al., 2003).

Study of the impact of hairpin RNA-mediated silencing and VIGS of HCT in Arabidopsis and *N. benthamiana* plants, respectively, provided unequivocal proof of the involvement of HCT in lignin biosynthesis. HCT-silenced plants exhibited profound changes in plant development, lignin content, and structure and susceptibility of the cell walls to enzymatic degradation. Comparison of enzyme immunolocalization in control and silenced plants by confocal microscopy demonstrated a correlation between the disappearance of enzyme labeling in vascular cells and the impact on lignin structure. In silenced *N. benthamiana* plants, accumulation of the gene product in the cambium zone and in xylem ray cells was clearly diminished compared with controls. Cell walls of tissues that underwent silencing displayed surprisingly higher autofluorescence, suggesting that the enrichment of lignin in H units demonstrated after thioacetolysis may result in alterations of its spectral properties. This phenomenon could be linked to the fact that H lignin units are essentially terminal lignin units with free phenolic groups (Lange et al., 1995). The decrease in HCT protein accumulation in xylem tissues also strictly correlated with a decrease in lignin S unit content as revealed by histochemical staining and chemical analysis. The detailed analysis of HCT in different lignifying tissues and during plant development as a whole would be an interesting area for further research.

These changes in enzyme accumulation and lignin composition were unevenly distributed within the stem tissues of infected plants, suggesting some heterogeneity in the effects of silencing. Because VIGS was used to knock down HCT gene expression in *N. benthamiana*, the lignin heterogeneity may reflect the rate of replication and/or cell-to-cell spread of the TRV-HCT vector because it is known that the efficiency of VIGS is dependent on virus replication, at least at the stage of VIGS initiation (Ruiz et al., 1998). In TRV-infected plants, the virus multiplication rate is initially high, then declines and is maintained at a low level at later stages of infection (Ratcliff et al., 2001). The most important issue here is that HCT-targeted VIGS lead to a plant vasculature with a lignin that is unusual in its enrichment in H units, its depletion in S units, and its heterogeneous nature. Because VIGS is not uniform over the plant and does not eliminate HCT (Figure 8), late/partial silencing of HCT may result in effects specific to S lignin units. Moreover, it must be kept in mind that, in TRV-HCT infected plants, the new lignin built up after HCT silencing is added to wild-type lignin. A major advantage of VIGS over other

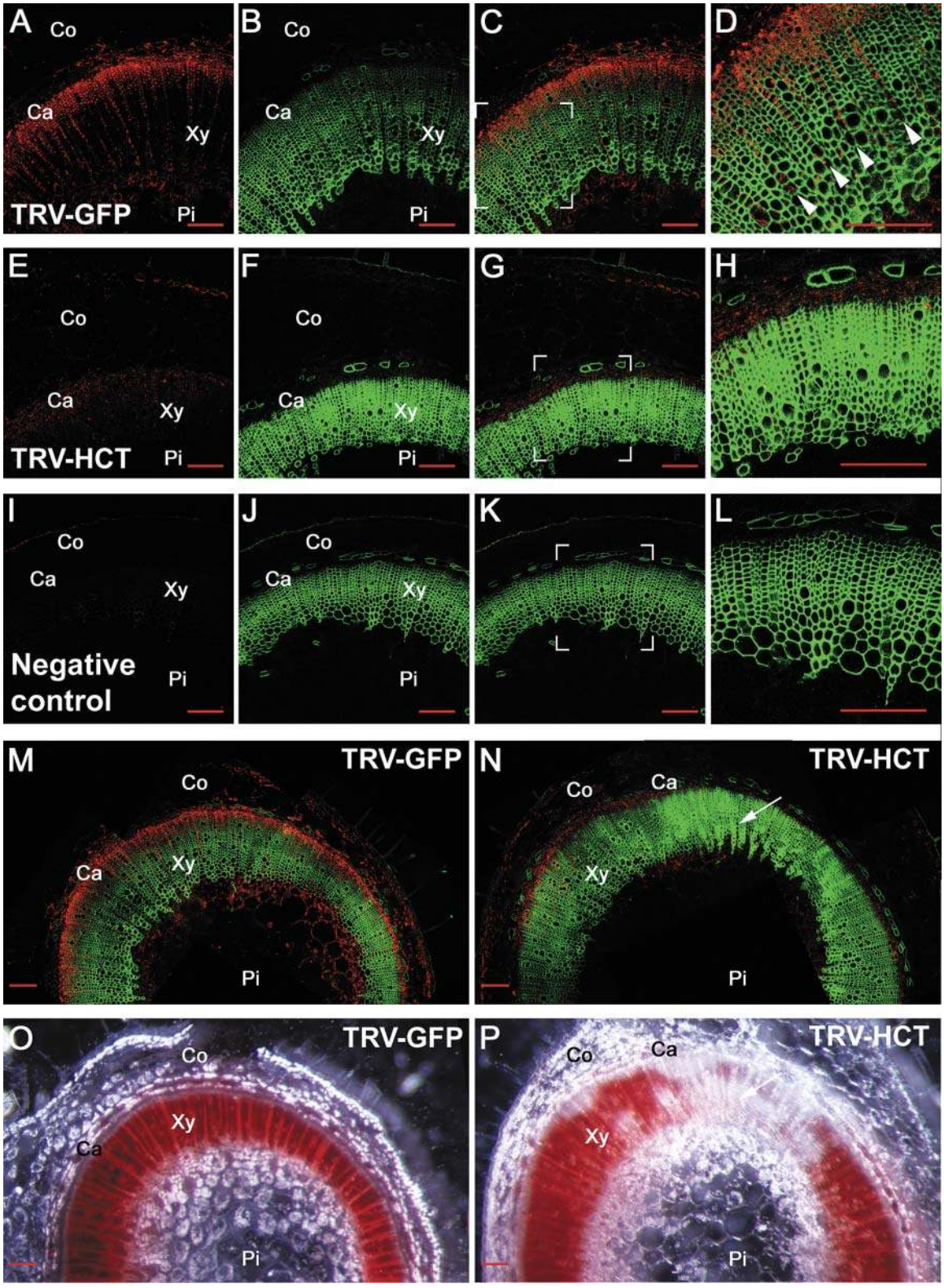

Figure 10. HCT Immunolocalization in Transverse Stem Sections from Control (TRV-GFP) and Silenced (TRV-HCT) *N. benthamiana* Plants.

(A) to **(D)** HCT immunolocalization in TRV-GFP control plants.

Table 2. Impact of *HCT* Silencing on Cell Wall Degradability by Cellulase

	Noninfected	TRV-GFP Infected	TRV-HCT Infected
Weight loss (%)	33.9 ± 0.7	36.7 ± 2.3	57.4 ± 1.4

The extent of degradation by cellulase was expressed as the percentage of loss in sample weight at the end of incubation with the enzyme (see Methods). Data are mean values and standard errors from duplicate experiments.

gene knockout systems is its conditional nature that allows repression of genes essential for plant growth (Lu et al., 2003). This is perfectly illustrated here by comparing the impact of HCT repression by VIGS and in the transgenic plants expressing the HCT hairpin construct.

It will be of interest to examine in depth the impact of abnormal lignin synthesis on cell differentiation. However, the currently available histochemical methods only allow detection of gross changes in lignin structure, whereas characterization of more subtle alterations, possibly affecting different cell types, would demand novel spectroscopic methods for in situ studies. It has been established that, during cell wall differentiation, patterns of lignification are well defined, leading to the overall architecture of the secondary cell wall. First, *p*-coumaryl alcohol is predominantly deposited into the middle lamella and cell corners (H unit, Figure 1) followed by coniferyl alcohol, which is mainly laid down in the secondary wall (G unit). Finally, sinapyl alcohol is deposited at the late stages of lignification (S unit) (Lewis, 1999). In HCT-silenced plants, the proportion of monolignols is modified, and resulting alterations in the cell wall ultrastructure could be studied, for instance, by immunogold labeling of lignin substructure epitopes using transmission electron microscopy (Ruel et al., 2001). Such approaches should improve our knowledge of the precise spatio-temporal regulation of the secondary cell wall assembly.

A rather surprising finding reported here is the differential effect of HCT repression on G and S lignin units, which are both downstream of HCT (Figure 1). Aside from the unlikely occurrence of an alternative pathway, the predominant effect on S synthesis suggests that, when the metabolic flux is lowered by HCT repression, the reduction of coniferaldehyde into coniferyl alcohol and polymerization in guaiacyl lignin is favored versus hydroxylation and methylation leading to syringyl lignin (Figure 1). Such a channeling mechanism could be demonstrated by feeding labeled precursors and following label fate in the intermediate pools.

Regulation of caffeoylquinate pools upon changes in activity of an upstream enzyme like Phe ammonia-lyase (Maher et al., 1994; Howles et al., 1996) or a downstream enzyme like cinnamoyl-CoA reductase (Chabannes et al., 2001) has been reported previously. Here, the analysis of the impact of HCT silencing on soluble phenylpropanoids of stems and leaves by HPLC revealed unexpected differential effects in the two organs; that is, an increase of caffeoylquinate pools in stems and no significant change of the same compounds in leaves. However, these phenomena may have different origins. First of all, and though HCT has been shown to synthesize caffeoylquinate in vitro (Hoffmann et al., 2003), it is possible that another acyltransferase, which has been characterized recently in tobacco and tomato (*Lycopersicon esculentum*) (C. Martin, personal communication), is involved in caffeoylquinate biosynthesis in leaves. Moreover, it is known that HCT is involved both upstream and downstream of the 3-hydroxylation step (Figure 1). Thus, HCT inhibition in stems could affect predominantly caffeoylquinate catabolism into caffeoyl CoA, leading to caffeoylquinate accumulation. Another possibility is that distinct pools of caffeoylquinate occur: one metabolically active that predominates in stems and is highly responsive to changes in HCT activity and another pool that is quantitatively important in leaves and is slowly mobilized. In addition, although the transport of phenylpropanoids through the plant has not been demonstrated, it could also contribute to the observed differences between organs. It is evident that these possibilities are not

Figure 10. (continued).

(E) to **(H)** HCT immunolocalization in HCT-silenced plants.

(I) to **(L)** Negative control. Labeling was performed on TRV-GFP plants in the absence of primary antibodies.

(A), **(E)**, and **(I)** Typical distribution of the HCT immunolabeling. HCT labeling is intense and mainly detected within the cambium (Ca) of the TRV-GFP sample. Strongly reduced labeling is observed in the cambium of the HCT-silenced tissues. Almost no signal is detected in the negative control.

(B), **(F)**, and **(J)** Corresponding autofluorescence of the lignin as observed upon 488/505 to 545 nm excitation/emission wavelengths. Note that autofluorescence of the lignin is higher and less uniformly distributed in the HCT-silenced tissues **(F)** compared with the TRV-GFP infected tissues (**[B]** and **[J]**).

(C), **(G)**, and **(K)** Merged images of **(A)** + **(B)**, **(E)** + **(F)**, and **(I)** + **(J)**, respectively.

(D), **(H)**, and **(L)** Higher magnification views of the boxed regions shown in **(C)**, **(G)**, and **(K)**, respectively. Note the HCT labeling within the xylem ray cells of TRV-GFP plants (arrowheads).

(M) and **(N)** Overall distribution of HCT protein (red) and lignin (green) in transverse stem sections from TRV-GFP and TRV-HCT–infected *N. benthamiana*.

(O) and **(P)** Maüle staining corresponding to the samples shown in **(M)** and **(N)**, respectively. Note that the unstained area of the xylem shows a higher level of autofluorescence (arrows).

All images were acquired by CLSM and processed under exactly the same conditions to allow comparison between the different panels. Bars = 200 μm. Abbreviations are as in Figures 4 and 9.

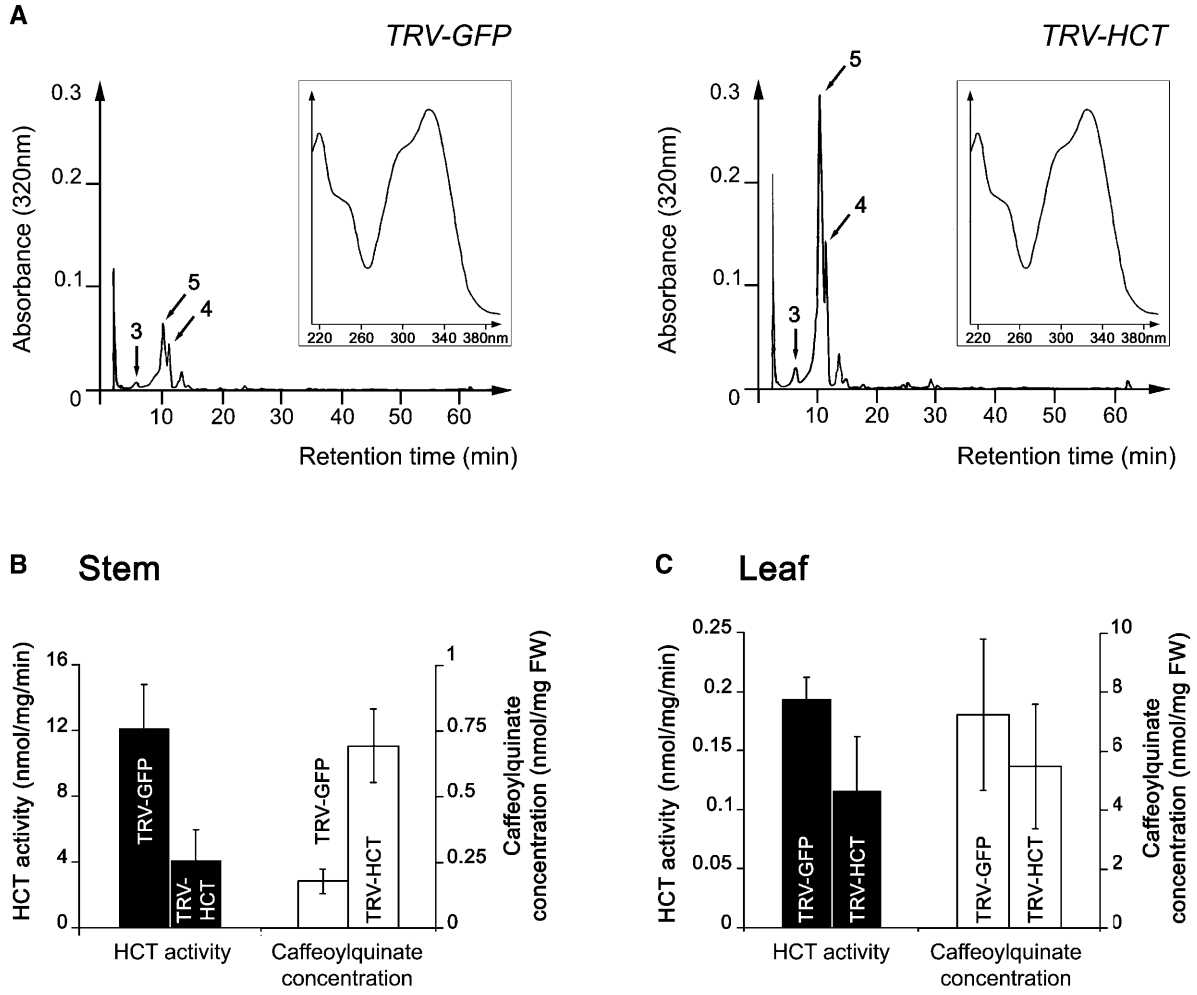

Figure 11. Impact of *HCT* Silencing on the Accumulation of Soluble Phenolic Compounds in *N. benthamiana*.

(A) Phenolic compounds extracted from stems of TRV-GFP or TRV-HCT–infected *N. benthamiana* plants were separated by HPLC. The three major peaks of each profile had the same UV spectrum (shown in the insets) that is characteristic of caffeoylquinate isomers (3-, 4-, and 5- isomers as indicated).

(B) and **(C)** Mean values of HCT activity and caffeolquinate content measured in the same samples of stem **(B)** and leaf **(C)** tissues. Nine TRV-GFP and TRV-HCT–infected plants were individually analyzed. FW, fresh weight.

exclusive and tracer experiments with labeled precursors should clarify their relative importance. Finally, one cannot completely rule out that VIGS has differently affected stem and leaf tissues of the plant because of differences in viral replication efficiency.

Recently, major advances have been made in the understanding of the phenylpropanoid pathway by analyzing the impact of lignin biosynthetic gene repression in antisense plants (Atanassova et al., 1995; Chabannes et al., 2001; Pinçon et al., 2001a, 2001b; Abbott et al., 2002; Boerjan et al., 2003) and Arabidopsis mutants (Franke et al., 2002b; Humphreys and Chapple, 2002; Boerjan et al., 2003; Goujon et al., 2003). Depending on the enzyme targeted for repression, different changes in lignin content and/or composition were observed, and these findings have shed new light on the role of the targeted enzymatic step in the biosynthetic pathway. For example, the strong reduction of S units in the lignin of transgenic tobacco with reduced COMT I activity demonstrated the function of COMT I in S unit synthesis and implicated CCoAOMT in G unit synthesis (Atanassova et al., 1995) (Figure 1). The role of CCoAOMT has been confirmed by analysis of new antisense plants (Pinçon et al., 2001a). It should be noted that, in most of the aforesaid cases and in others, changes in guaiacyl and/or syringyl unit synthesis were observed, resulting in variations in the S/G ratio but not systematically in detectable changes of lignin content, nor was the H unit content affected, angiosperm lignin being mainly constituted of G and S units. As shown in Figure 1, the conversion of the metabolic precursor of the H unit, *p*-coumaroyl CoA, into caffeoyl CoA (the precursor of both G and S lignin units) is catalyzed sequentially by HCT and C3H. Recently, it was shown that an Arabidopsis mutant (*ref8*) obtained by ethyl methanesulfonate mutagenesis is affected in the *C3H* gene. The mutant displayed a dwarf phenotype and contained less lignin than wild-type

plants. Its lignin was unusual in being composed primarily of H units (Franke et al., 2002b). T-DNA insertion mutant lines tagged in the *C3H* gene have also been isolated (D. Werck-Reichhart, personal communication) and display even more drastic growth defects. Our HCT-silenced Arabidopsis plants also have a very severe growth phenotype reminiscent of that of the *C3H*-tagged mutants and a lignin depleted in S unit as demonstrated by the negative response to Maüle reagent (Figure 5). Lignin of TRV-HCT–infected *N. benthamiana* was analyzed by thioacidolysis and showed the same changes compared with wild-type lignin as those reported for the *ref8* mutant, although to a lesser extent, probably because (1) HCT silencing by VIGS was induced at an advanced stage of development (i.e., after wild-type lignin was formed) and (2) as discussed above, all infected cells were probably not affected to the same extent. The comparable phenotypes observed for plants affected in the *C3H* or *HCT* genes are consistent with the fact that *C3H* and *HCT* genes have similar expression profiles (Raes et al., 2003), and the two enzymatic steps are consecutive in the synthesis of caffeoyl CoA from *p*-coumaroyl CoA. The mutant phenotypes may be related to the growth-promoting activity that has been shown for some phenylpropanoids, such as dehydrodiconiferyl alcohol glucoside (Binns et al., 1987). Furthermore, the modifications of lignin structure and content decreased cell wall resistance to hydrolytic enzymes of the Arabidopsis mutant *ref8* as observed for the HCT-silenced *N. benthamiana* plants described here. These data point to the importance of lignification for cell wall resistance to the action of hydrolytic enzymes, such as those produced by pathogenic organisms. The study of the resistance of silenced plants to bacterial and fungal pathogens will enable us to test this hypothesis.

METHODS

Chemicals, Enzymes, and General Methods

Commonly used chemicals and reagents were of the highest purity readily available. Bradford protein dye reagent was purchased from Bio-Rad (Hercules, CA). Restriction enzymes and buffers were purchased from New England Biolabs (Beverly, MA) or Invitrogen (Cergy Pontoise, France). T4 DNA ligase, T4 polynucleotide kinase, and ATP were purchased from Invitrogen. Purified oligonucleotides used for cloning and DNA sequencing were provided by Sigma-Aldrich (Saint-Quentin-Fallavier, France). DNA amplification using *Taq* polymerase (Invitrogen) was performed in the iCycler thermocycler (Bio-Rad). Plasmid and PCR products were extracted and purified from agarose gels using kits purchased from Qiagen (Hilden, Germany).

Plant Material and Culture Conditions

Nicotiana tabacum and *N. benthamiana* plants were grown in a growth chamber under 3000 lux lighting and a light/dark cycle of 16 h/8 h. The temperature was maintained at 21 ± 2°C. Tissues were harvested from flowering tobacco plants and frozen in liquid nitrogen. One-month-old *N. benthamiana* seedlings were infected with TRV constructs using *Agrobacterium tumefaciens*–mediated transient gene expression (Ratcliff et al., 2001).

Arabidopsis thaliana plants ecotype Columbia 0 were grown with a light/dark cycle of 12 h/12 h and a temperature of 20°C during the day and 16°C at night.

DNA Sequencing

DNA sequencing was performed by the method of Sanger et al. (1977) using the rhodamine dye-terminator cycle ready kit with AmpliTaq DNA polymerase FS (Perkin-Elmer, Foster City, CA) and an Applied Biosystems DNA sequencer (Model 373A; Foster City, CA).

Production and Use of Polyclonal Antibodies

Heterologous expression in *Escherichia coli* cells and purification of the HCT protein were performed as described previously (Hoffmann et al., 2003). Polyclonal antibodies were raised in rabbit by four successive injections of 100 μg of the purified enzyme. Before injection, the protein solution was emulsified with Freund's complete adjuvant for the first injection and with incomplete adjuvant for the others. The anti-CCoAOMT antibodies were produced as described (Maury et al., 1999). Anti-HCT antibodies were used at 1/10,000 or 1/500 dilution and anti-CCoAOMT serum at 1/2000 or 1/200 dilution in protein gel blot and immunohistochemical analyses, respectively.

For specificity tests, anti-HCT antibodies were preincubated for 2 h at 20°C in PBS or in PBS containing 100 or 500 μM of purified HCT recombinant protein in protein gel blot or immunohistochemical analyses, respectively.

For immunoprecipitation experiments, 8 mg of protein A–Sepharose CL-4B beads (Sigma, St. Louis, MO), prewashed twice with 40 μL of PBS buffer for 4 h at 4°C, was centrifuged at 1000 rpm for 5 min, resuspended in 40 μL of 1 M sodium phosphate buffer, pH 7.5, and incubated for 3 h at 4°C in the presence of 5 μL of anti-HCT or preimmune serum. The beads were incubated overnight at 4°C with 200 μL of crude protein extracts and then centrifuged at 2000 rpm for 5 min. The supernatant was assayed for HCT activity. Control incubations were performed in the absence of protein A–Sepharose and antibody. Four independent measurements were performed in each case.

Protein Gel Blot Analysis

The basic procedures for electrophoresis of proteins under denaturing conditions and immunoblotting were as described previously (Geoffroy et al., 1990), except that phosphatase activity was detected with a chemiluminescent substrate (BioRad CDP-Star).

DNA Gel Blotting

Genomic DNA analysis was performed as previously described by Martz et al. (1998). DNA samples (40 μg) were digested to completion with one or two restriction enzymes, ethanol-precipitated, and resolved on 0.8% agarose gel. After depurination, the gel was blotted on Hybond N+ membrane (Amersham Bioscience, Orsay, France). The [α-^{32}P]dCTP-labeled probe was synthesized from the 957-bp *N. benthamiana* HCT fragment by random priming. DNA gel blot hybridization and washing steps were performed at 65°C. Hybridization signals were detected by phosphorimaging.

RNA Gel Blot Analysis

Total RNA extraction was performed with Tri-Reagent (Sigma), and analysis of high and low molecular weight RNA was as described (Himber et al., 2003). dCTP-labeled probe was synthesized from the 367-bp Arabidopsis HCT fragment (see below) by random priming. All hybridization signals were detected by phosphorimaging.

HCT Activity Assays

Plant tissues were ground with a pestle and mortar in liquid nitrogen, and the powder was extracted with 0.1 M sodium phosphate buffer, pH 7.5,

containing 10 mM DTT, quartz, and polyclar AT (Serva, Buchs, Switzerland). After centrifugation at 4°C for 20 min at 13,000 rpm, the supernatant was washed twice with the extraction buffer on Centricon 10 concentrators (Amicon, Ranvers, MA) to eliminate soluble phenolic compounds present in the crude extract and then used for HCT activity measurement. The reaction mixture contained 100 mM phosphate buffer, pH 6.6, 1 mM DTT, 0.4 to 12 μg of protein, 100 μM *p*-coumaroyl CoA, and 4 mM shikimate in a total volume of 20 μL. The reaction was initiated by addition of the enzyme extract, incubated at 30°C for 2 to 30 min, and terminated by addition of 20 μL of HPLC solvent. Reaction products were analyzed and quantified by HPLC. Protein content was measured by the Bradford method (Bradford, 1976).

Immunohistochemical Analyses

Stems from 8-week-old *N. tabacum* were collected, fixed with a solution containing 3.7% formaldehyde, 50% ethanol, and 5% acetic acid in water, dehydrated in an ethanol series, and embedded in paraplast before 10-μm-thick sections were made. Stems of 8-week-old *N. benthamiana* infected for 4 weeks were hand-sectioned and immediately fixed for 1 h by immersion in ethanol. Before immunolabeling, sections were rehydrated in PBS solution, blocked for 1 h in PBS containing 5% (w/v) BSA, 5% (v/v) normal goat serum, and 0.1% cold water fish skin gelatine (Aurion, Wageningen, The Netherlands), and further incubated overnight at 4°C in PBS containing 0.1% (v/v) acetylated BSA (Aurion). Sections were then washed four times in PBS and incubated again in the dark for 4 h at room temperature with Alexa Fluor 568 goat anti-rabbit immunoglobulin G (Alexa 568; Molecular Probes, Leiden, The Netherlands) diluted 1:300 in PBS plus 0.1% acylated BSA. Samples were washed again four times before light microscopy observations. Control experiments in which primary antibodies were omitted were routinely performed to verify the specificity of the labeling. Controls using antibodies preincubated with the recombinant HCT protein were performed on ethanol-fixed sections (see supplemental data online).

Epifluorescence Microscopy

Epifluorescence microscopy observations were done with a Nikon Eclipse E800 microscope (Champigny sur Marne, France) with appropriate filters and an ×10 0.3–numerical aperture objective. For Alexa 568, the parameters were as follows: excitation wavelength, 515 to 565 nm; dichroic mirror, 565 nm; and emission bandpass filter, 582.5 to 627.5 nm. For lignin autofluorescence, the parameters were as follows: excitation wavelength, 330 to 380 nm; dichroic mirror, 400 nm; and emission longpass filter, 420 nm. Image acquisition was performed as previously described (Gaire et al., 1999).

CLSM

CLSM was performed with a Zeiss LSM510 microscope (Jena, Germany) equipped with a Zeiss Axiovert 100M inverted microscope and a ×10 0.3–numerical aperture objective. Laser scanning was performed using the multitrack mode to avoid bleed-through. Excitation/emission wavelengths were 488/505 to 545 nm for lignin and 543/560 to 615 nm for Alexa 568. Image processing used LSM510 version 2.8 (Zeiss) and PhotoShop 5.5 (Adobe Systems, San Jose, CA) for final assembly.

RNA Silencing in Arabidopsis

A 367-bp HCT fragment was PCR amplified from the pGEX-KG plasmid containing the Arabidopsis *HCT* gene (At5g48930) (Hoffmann et al., 2003). The sense and antisense primer sequences were 5′-GAGTCTAGACTCGAGGTAACGCCGAGGGAGTGGAA-3′ and 5′-CATGGATCCGGCGCGCCAGAAATGGAACGGTTTCTAACG-3′, respectively. The resulting PCR product was inserted into pFGC5941 (www.ag.arizona.edu/chromatin/fgc5941.html), a binary vector containing a chalcone synthase intron and designed to produce double-stranded RNA in plants. The *HCT* gene fragment was cloned upstream and downstream of the chalcone synthase intron in sense and antisense orientation using *Xho*I-*Asc*I and *Xba*I-*Bam*HI restriction sites, respectively. Transformation of Arabidopsis (Columbia 0) was performed with Agrobacterium GV3101 strain as described previously (Bechtold et al., 1993). Transgenic plants were selected by spraying a 300-mg/L solution of Basta (glufosinate) herbicide.

Cloning of a Partial HCT cDNA from *N. benthamiana*

Reverse Transcription

Reverse transcription with total RNA from 1-month-old N. benthamiana stems was performed using (poly)dT primer and Superscript (Life Technologies) according to the manufacturer's instructions.

Generation of Partial cDNAs

Partial cDNAs were produced by PCR using as template the cDNA generated by reverse transcription. The sense degenerate oligonucleotide primer (5′-TTTTAYCCNATGGCKGGKMG-3′) was based on the consensus sequence FYPMAG conserved between N. tabacum HCT and other acyltransferases (Hoffmann et al., 2003). The antisense primer was based upon the conserved region DFGWG near the C terminus of acyltransferase proteins and had the following sequence: 5′-CCCCAICCRAARTC-3′. I indicates inosine and R, H, Y, K, M, and N indicate the following degenerate sites: R, A/G; H, A/C/T; Y, C/T; K, G/T; M, A/C; and N, A/G/C/T. DNA amplification was performed under the following conditions: 3 min at 94°C and then 35 cycles at 94°C for 1 min, 42°C for 1 min, and 72°C for 1 min. At the end of the 35 cycles, the reaction mixture was incubated for an additional 10 min at 72°C. The amplified DNA was resolved by agarose gel electrophoresis, and the band of the correct size (957 bp) was isolated and subcloned into pCRII-TOPO (Invitrogen) before sequencing.

VIGS Technology

VIGS technology was used to induce HCT gene silencing in *N. benthamiana* with the tobacco rattle virus vector system (Ratcliff et al., 2001). The 957-bp cDNA fragment of the *N. benthamiana* HCT gene was cloned into the *Apa*I and *Bam*HI sites of pTV00 vector to produce the pTV-HCT construct used for *N. benthamiana* infection.

Lignin Analysis

Histochemical analysis using Wiesner and Maüle staining was performed as previously described (Atanassova et al., 1995). In the case of Arabidopsis plants, 2-month-old silenced or wild-type stems were embedded in 1% low melting point agarose before to be sectioned transversally with a razor blade. The observations were performed with a Nikon TE2000 inverted microscope.

Lignin chemical analysis was performed on the stems of 3-month-old *N. benthamiana* plants (~20 plants per sample) that had been infiltrated 8 weeks before collection. The air-dried stems were evenly ground to pass through a 0.5-mm sieve before an exhaustive solvent extraction, first with toluene:ethanol (2:1, v/v), then with ethanol, and finally with water. As recommended in the standard method of Klason lignin determination, this comprehensive extraction step was performed to minimize the possibility that proteinaceous components are included within the so-called Klason lignin fraction (Dence, 1992). The Klason lignin content was calculated in weight percent of the dry extract-free stem material and from four

replicates performed on 300 mg of sample. Thioacidolysis reagent was prepared by introducing 2.5 mL of BF_3 etherate (Sigma-Aldrich) and 10 mL of ethanethiol EtSH (Sigma-Aldrich) into a 100-mL flask and adjusting the final volume to 100 mL with dioxane. The colorless reagent was used immediately after preparation. The extract-free stem samples (20 mg) were added to 10 mL of reagent and 1 mL of solution of GC internal standard (docosane, 0.24 mg/mL in CH_2Cl_2) in a glass tube closed with a Teflon-lined screwcap. Thioacidolysis was performed at 100°C in an oil bath for 4 h. The cooled reaction mixture was diluted with 30 mL of water, and the pH was adjusted to 3 to 4 with 0.4 M $NaHCO_3$. The reaction mixture was extracted with CH_2Cl_2 (3 × 30 mL). Combined organic extracts were dried over Na_2SO_4 and then evaporated under reduced pressure at 40°C. The final residue was redissolved in ~0.5 mL of CH_2Cl_2 before silylation and gas chromatography–mass spectrometry analyses according to Lapierre (1986). Quantitation of the main *p*-hydroxyphenyl (H), guaiacyl (G), and syringyl (S) lignin-derived monomers, analyzed as their trimethylsilylated derivatives, was performed from specific ion chromatograms reconstructed at m/z 239 for the H monomers, 269 for G monomers, and at m/z 299 for S monomers after an appropriate calibration relative to the docosane internal standard.

Cell Wall Degradability

The susceptibility to cellulolysis was evaluated using a method adapted from Rexen (1977): 200 mg of the extract-free ground sample were placed in 30 mL of 0.05 M sodium acetate buffer, pH 4.5, containing 2 mg/mL of commercial cellulase (cellulase Onozuka-R10; Serva, Heidelberg, Germany). The cellulolysis was performed for 48 h at 37°C with magnetic stirring. After incubation, the reaction medium was filtrated over a tared filtering crucible and the residue was washed with water, oven-dried, and then gravimetrically determined.

Extraction of Soluble Phenolic Compounds from Plant Material

Samples (100 mg) from TRV-GFP and TRV-HCT plants were frozen in liquid nitrogen and quickly ground in 500 μL of methanol. After centrifugation at 500 rpm for 5 min, the supernatant was collected and the residual pellet was reextracted with 200 μL of 70% methanol. The supernatants were combined, clarified at 2000 rpm for 30 min, and taken to dryness under nitrogen. The dried material was dissolved in 70% methanol (300 μL) and analyzed by HPLC.

HPLC Analysis of HCT Reaction Products and Plant Phenolic Compounds

Phenolic compounds were resolved on a RP C18 column (Novapak, 4 μm, 4.6 × 250 mm; Waters, Milford, MA) using an increasing gradient of acetonitrile in water containing 0.1% formic acid. Gradient conditions at 1 mL/min flow rate were as follows: 100% solvent A to 50% solvent B for 50 min; 50% solvent B to 100% solvent B for 5 min; 100% solvent B to 100% solvent A for 5 min and then 10 min reequilibration in 100% solvent A. Solvent A contained acetonitrile/water/formic acid (10:89.9:0.1) and solvent B acetonitrile/water/formic acid (80:19.9:0.1). Compounds were characterized by their elution time, and their UV absorption spectrum recorded with a photodiode array detector (Waters). 3-*O*- and 4-*O*-caffeoylquinic acids were produced from 5-*O*-caffeoylquinic acid (Sigma-Aldrich) by heating for 30 min at 90°C in 0.2 M phosphate buffer, pH 7.0 (Strack and Gross, 1990), and the three isomers were separated by HPLC.

Synthesis and Purification of the *p*-Coumaroyl-CoA Substrate

p-Coumaroyl-CoA ester was prepared according to the method of Stöckigt and Zenk with some modifications (Stöckigt and Zenk, 1975; Negrel and Smith, 1984) and identified and quantified by spectroscopy.

Sequence data from this article have been deposited with the EMBL/GenBank data libraries under accession numbers AJ507825 for *N. tabacum* HCT cDNA and AJ555865 for *N. benthamiana* partial HCT cDNA.

ACKNOWLEDGMENTS

We wish to thank Robert Erb, Jérome Mutterer, and Matthieu Erhardt for assistance with microscopy, Frédéric Legée (Institut National de la Recherche Agronomique) for the Klason lignin determinations, Phil Mullineau (John Innes Centre, Norwich) for pSoup plasmid, David Baulcombe (John Innes Centre) for VIGS vectors, and Danielle Werck-Reichhart (Institut de Biologie Moléculaire des Plantes) and Cathie Martin (John Innes Centre) for sharing unpublished data. The assistance of Laurette De Franco is gratefully acknowledged. We are indebted to Patrice Dunoyer, Christophe Himber, and Charles Lecellier for technical support and valuable suggestions about RNA silencing experiments. We are grateful to Kenneth Richards and Olivier Voinnet for critical reading. The Zeiss LSM510 confocal microscope was cofinanced by the Centre National de la Recherche Scientifique, the Université Louis Pasteur, the Région Alsace, the Association de la Recherche sur le Cancer, and the Ligue Nationale contre le Cancer.

Received December 19, 2003; accepted March 10, 2004.

REFERENCES

Abbott, J.C., Barakate, A., Pinçon, G., Legrand, M., Lapierre, C., Mila, I., Schuch, W., and Halpin, C. (2002). Simultaneous suppression of multiple genes by single transgenes. Down-regulation of three unrelated lignin biosynthetic genes in tobacco. Plant Physiol. **128,** 844–853.

Atanassova, R., Favet, N., Martz, F., Chabbert, B., Thollier, M.T., Monties, B., Fritig, B., and Legrand, M. (1995). Altered lignin composition in transgenic tobacco expressing O-methyltransferase sequences in sense and antisense orientation. Plant J. **8,** 465–477.

Bandoniene, D., and Murkovic, M. (2002). On-line HPLC-DPPH screening method for evaluation of radical scavenging phenols extracted from apples (*Malus domestica* L.). J. Agric. Food Chem. **50,** 2482–2487.

Bechtold, N., Ellis, J., and Pelletier, G. (1993). In planta *Agrobacterium*-mediated gene transfer by infiltration of adult *Arabidopsis thaliana* plants. C. R. Acad. Sci. III Sci. Vie **316,** 1194–1199.

Binns, A.N., Chen, R.H., Wood, H.N., and Lynn, D.G. (1987). Cell division promoting activity of naturally occurring dehydrodiconiferyl glucosides: Do cell wall components control cell division? Proc. Natl. Acad. Sci. USA **84,** 980–984.

Boerjan, W., Ralph, J., and Baucher, M. (2003). Lignin biosynthesis. Annu. Rev. Plant Biol. **54,** 519–546.

Boveris, A., Valdes, L., and Alvares, S. (2002). Inhibition by wine polyphenols of peroxynitrite-initiated chemiluminescence and NADH oxidation. Ann. N. Y. Acad. Sci. **957,** 90–102.

Bradford, M.M. (1976). A rapid and sensitive method for the quantitation of microgram quantities of protein utilizing the principle of protein-dye binding. Anal. Biochem. **72,** 248–254.

Burns, J., Gardner, P., O'Neil, J., Crawford, S., Morecroft, I., McPhail, D., Lister, C., Matthews, D., MacLean, M., Lean, M., Duthie, G., and Crozier, A. (2000). Relationship among antioxidant activity, vasodilation capacity and phenolic content of red wines. J. Agric. Food Chem. **48,** 220–230.

Chabannes, M., Barakate, A., Lapierre, C., Marita, J.M., Ralph, J., Pean, M., Danoun, S., Halpin, C., Grima-Pettenati, J., and Boudet, A.M. (2001). Strong decrease in lignin content without significant alteration of plant development is induced by simultaneous down-regulation of cinnamoyl CoA reductase (CCR) and cinnamyl alcohol dehydrogenase (CAD) in tobacco plants. Plant J. **28,** 257–270.

Croteau, R., Kutchan, T.M., and Lewis, N.G. (2000). Natural products (secondary metabolites). In Biochemistry and Molecular Biology of Plants, B.B. Buchanan, W. Gruissem, and R.L. Jones, eds (Rockville, MD: American Society of Plant Physiologists), pp. 1250–1318.

Dence, C. (1992). The determination of lignin. (Berlin: Springer-Verlag).

Dixon, R.A., and Ferreira, D. (2002). Genistein. Phytochemistry **60,** 205–211.

Franke, R., Hemm, M.R., Denault, J.W., Ruegger, M.O., Humphreys, J.M., and Chapple, C. (2002b). Changes in secondary metabolism and deposition of an unusual lignin in the *ref8* mutant of Arabidopsis. Plant J. **30,** 47–59.

Franke, R., Humphreys, J.M., Hemm, M.R., Denault, J.W., Ruegger, M.O., Cusumano, J.C., and Chapple, C. (2002a). The Arabidopsis REF8 gene encodes the 3-hydroxylase of phenylpropanoid metabolism. Plant J. **30,** 33–45.

Gaire, F., Schmitt, A.C., Stussi-Garaud, C., Pinck, L., and Ritzenthaler, C. (1999). Protein 2A of grapevine fanleaf nepovirus is implicated in RNA2 replication and colocalizes to the replication site. Virology **264,** 25–36.

Geoffroy, P., Legrand, M., and Fritig, B. (1990). Isolation and characterization of a proteinaceous inhibitor of microbial proteinases induced during the hypersensitive reaction of tobacco to tobacco mosaic virus. Mol. Plant-Microbe Interact. **3,** 327–333.

Goujon, T., Sibout, R., Pollet, B., Maba, B., Nussaume, L., Bechtold, N., Lu, F., Ralph, J., Mila, I., Barriere, Y., Lapierre, C., and Jouanin, L. (2003). A new Arabidopsis thaliana mutant deficient in the expression of O-methyltransferase impacts lignins and sinapoyl esters. Plant Mol. Biol. **51,** 973–989.

Heller, W., and Kuhnl, T. (1985). Elicitor induction of a microsomal 5-O-(4-coumaroyl)shikimate 3′-hydroxylase in parsley cell suspension cultures. Arch. Biochem. Biophys. **241,** 453–460.

Himber, C., Dunoyer, P., Moissiard, G., Ritzenthaler, C., and Voinnet, O. (2003). Transitivity-dependent and -independent cell-to-cell movement of RNA silencing. EMBO J. **22,** 4523–4533.

Hoffmann, L., Maury, S., Martz, F., Geoffroy, P., and Legrand, M. (2003). Purification, cloning and properties of an acyltransferase controlling shikimate and quinate ester intermediates in phenylpropanoid metabolism. J. Biol. Chem. **278,** 95–103.

Howles, P.A., Sewalt, V., Paiva, N.L., Elkind, Y., Bate, N.J., Lamb, C., and Dixon, R.A. (1996). Overexpression of L-phenylalanine ammonia-lyase in transgenic tobacco plants reveals control points for flux into phenylpropanoid biosynthesis. Plant Physiol. **112,** 1617–1624.

Humphreys, J.M., and Chapple, C. (2002). Rewriting the lignin roadmap. Curr. Opin. Plant Biol. **5,** 224–229.

Inoue, K., Sewalt, V.J.H., Ballance, G.M., Ni, W., Stürtzer, C., and Dixon, R.A. (1998). Developmental expression and substrate specificities of alfalfa caffeic acid 3-*O*-methyltransferase and caffeoyl-coenzyme A 3-*O*-methyltransferase in relation to lignification. Plant Physiol. **117,** 761–770.

Jang, M., Cai, L., Udeani, G., Slowing, K., Thomas, C., Beecher, C., Fong, H., Farnsworth, N., Kinghorn, A., Mehta, R., Moon, R., and Pezzuto, J. (1997). Cancer chemopreventive activity of resveratrol, a natural product derived from grapes. Science **275,** 218–220.

Kahkonen, M., Hopia, A., Vuorela, H., Rauha, J., Pihlaja, K., Kujala, T., and Heinonen, M. (1999). Antioxidant activity of plant extracts containing phenolic compounds. J. Agric. Food Chem. **47,** 3954–3962.

Kuhnl, T., Koch, U., Heller, W., and Wellmann, E. (1987). Chlorogenic acid biosynthesis: Characterization of a light-induced microsomal 5-O-(4-coumaroyl)-D-quinate/shikimate 3′-hydroxylase from carrot (Daucus carota L.) cell suspension cultures. Arch. Biochem. Biophys. **258,** 226–232.

Lange, B.M., Lapierre, C., and Sandermann, H., Jr. (1995). Elicitor-induced spruce stress lignin. Structural similarity to early developmental lignins. Plant Physiol. **108,** 1277–1287.

Lapierre, C. (1986). Thioacidolysis of poplar lignins: Identification of monomeric syringyl products and characterization of guaiacyl-syringyl rich fractions. Holzforschung **40,** 113–118.

Lekse, J.M., Xia, L., Stark, J., Morrow, J.D., and May, J.M. (2001). Plant catechols prevent lipid peroxidation in human plasma and erythrocytes. Mol. Cell. Biochem. **226,** 89–95.

Lewis, N.G. (1999). A 20th century roller coaster ride: A short account of lignification. Curr. Opin. Plant Biol. **2,** 153–162.

Lu, R., Martin-Hernandez, A.M., Peart, J.R., Malcuit, I., and Baulcombe, D.C. (2003). Virus-induced gene silencing in plants. Methods **30,** 296–303.

Maher, E.A., Bate, N.J., Ni, W., Elkind, Y., Dixon, R.A., and Lamb, C.J. (1994). Increased disease susceptibility of transgenic tobacco plants with suppressed levels of preformed phenylpropanoid products. Proc. Natl. Acad. Sci. USA **91,** 7802–7806.

Martz, F., Maury, S., Pinçon, G., and Legrand, M. (1998). cDNA cloning, substrate specificity and expression study of tobacco caffeoyl-CoA 3-O-methyltransferase, a lignin biosynthetic enzyme. Plant Mol. Biol. **36,** 427–437.

Maury, S., Geoffroy, P., and Legrand, M. (1999). Tobacco *O*-methyltransferases involved in phenylpropanoid metabolism: The different CCoAOMT and COMT classes have distinct substrate specificities and expression patterns. Plant Physiol. **121,** 215–224.

Negrel, J., and Smith, T.A. (1984). The phosphohydrolysis of hydroxycinnamoyl-CoA thioesters in plant extracts. Phytochemistry **23,** 31–34.

Olthof, M.R., Hollman, P.C., and Katan, M.B. (2001). Chlorogenic acid and caffeic acid are absorbed in humans. J. Nutr. **131,** 66–71.

Pinçon, G., Chabannes, M., Lapierre, C., Pollet, B., Ruel, K., Joseleau, J.-P., Boudet, A.M., and Legrand, M. (2001b). Simultaneous down-regulation of caffeic/5-hydroxyferulic acid-O-methyltransferase I and cinnamoyl-coA reductase in the progeny from a cross between tobacco lines homozygous for each transgene. Consequences for plant development and lignin synthesis. Plant Physiol. **126,** 145–155.

Pinçon, G., Maury, S., Hoffmann, L., Geoffroy, P., Lapierre, C., Pollet, B., and Legrand, M. (2001a). Repression of *O*-methyltransferase genes in transgenic tobacco affects lignin synthesis and plant growth. Phytochemistry **57,** 1167–1176.

Raes, J., Rohde, A., Christensen, J.H., Van De Peer, Y., and Boerjan, W. (2003). Genome-wide characterization of the lignification toolbox in Arabidopsis. Plant Physiol. **133,** 1051–1071.

Ratcliff, F., Martin-Hernandez, A.M., and Baulcombe, D.C. (2001). Tobacco rattle virus as a vector for analysis of gene function by silencing. Plant J. **25,** 237–245.

Rexen, B. (1977). Enzyme solubility: A method for evaluating the digestibility of alkali-treated straw. Anim. Feed Sci. Technol. **2,** 205–218.

Ruel, K., Chabannes, M., Boudet, A., Legrand, M., and Joseleau, J. (2001). Reassessment of qualitative changes in lignification of transgenic tobacco plants and their impact on cell wall assembly. Phytochemistry **57,** 875–882.

Ruiz, M.T., Voinnet, O., and Baulcombe, D.C. (1998). Initiation and maintenance of virus-induced gene silencing. Plant Cell **10,** 937–946.

Sanger, F., Nicklen, S., and Coulson, A.R. (1977). DNA sequencing with chain-terminating inhibitors. Proc. Natl. Acad. Sci. USA **74,** 5463–5467.

Schoch, G., Goepfert, S., Morant, M., Hehn, A., Meyer, D., Ullmann, P., and Werck-Reichhart, D. (2001). CYP98A3 from *Arabidopsis thaliana* is a 3′-hydroxylase of phenolic esters, a missing link in the phenylpropanoid pathway. J. Biol. Chem. **276,** 36566–36574.

Smith, N.A., Singh, S.P., Wang, M.B., Stoutjesdijk, P.A., Green, A.G., and Waterhouse, P.M. (2000). Total silencing by intron-spliced hairpin RNAs. Nature **407,** 319–320.

Stacewicz-Sapuntzakis, M., Bowen, P.E., Hussain, E.A., Damayanti-Wood, B.I., and Farnsworth, N.R. (2001). Chemical composition and potential health effects of prunes: A functional food? Crit. Rev. Food Sci. Nutr. **41,** 251–286.

Stöckigt, J., and Zenk, M.H. (1975). Chemical syntheses and properties of hydroxycinnamoyl-coenzyme A derivatives. Z. Naturforsch. **30,** 352–358.

St-Pierre, B., and De Luca, V. (2000). Evolution of acyltransferase genes: Origin and diversification of the BAHD superfamily of acyltransferase involved in secondary metabolism. Recent Adv. Phytochem. **34,** 285–315.

Strack, D., and Gross, W. (1990). Properties and activity changes of chlorogenic acid: Glucaric acid caffeoyltransferase from tomato (*Lycopersicon esculentum*). Plant Physiol. **92,** 41–47.

Ye, Z.-H. (1997). Association of caffeoyl coenzyme A 3-O-methyltransferase expression with lignifying tissues in several dicot plants. Plant Physiol. **115,** 1341–1350.